Marine Biodiversity (2022) 52: 52
https://doi.org/10.1007/s12526-022-01279-z

SENCKENBERG

ORIGINAL PAPER

Diversity and distribution of Kinorhyncha in abyssal polymetallic nodule areas of the Clarion-Clipperton Fracture Zone and the Peru Basin, East Pacific Ocean, with the description of three new species and notes on their intraspecific variation

Nuria Sánchez[1] · Alberto González-Casarrubios[1] · Diego Cepeda[1] · Sahar Khodami[2] · Fernando Pardos[1] · Annemiek Vink[3] · Pedro Martínez Arbizu[2]

Received: 1 October 2021 / Revised: 29 March 2022 / Accepted: 1 April 2022 / Published online: 14 September 2022

Abstract

Polymetallic nodule fields represent a large reservoir of undiscovered biodiversity that becomes particularly evident for meiobenthic organisms, the smallest-sized faunal group. Knowledge gaps are especially noticeable for the generally low-density metazoan groups, such as Kinorhyncha, the so-called mud dragons. Using both morphological and genetic (metabarcoding) approaches, we provide a general overview and comparison of the diversity of kinorhynchs collected during nine sampling campaigns (2016–2019) that targeted abyssal environments in several contract areas for exploration in the Clarion-Clipperton Fracture Zone (CCZ) and in the Peru Basin. Our findings from morphological analyses reveal a highly diverse mud dragon community, with 16 species present in the CCZ. Of these, 12 appear in the German contract area, including three new species described in the present contribution: *Echinoderes delaordeni* sp. nov., *Echinoderes sanctorum* sp. nov., and *Echinoderes zeppilliae* sp. nov. Furthermore, metabarcoding data of the kinorhynch community gathered from the area is provided, together with the geographic distribution of the known species stated per contractor area, including new records and still undescribed species. Most of the identified species in the CCZ seem to have a wide distribution, with *Echinoderes* sp.4 being the most common and abundant species with a distribution spreading across the CCZ and also present in the Peru Basin. Metabarcoding analyses targeting the V1V2 hypervariable region of the 18S gene from the 253 stations of the CCZ revealed 14 amplicon sequence variants (ASVs) belonging to Kinorhyncha with grade values higher than 98% detected at 15 different stations within six different areas along the CCZ. Concurring with morphology, the family Echinoderidae was the most diverse as the genus *Cephalorhyncha* had five ASVs, followed by *Echinoderes* with four ASVs. *Semnoderes*, however, showed the widest spread ASV, being detected at six stations. In the CCZ, the metabarcoding data showed there were no shared ASVs between the CCZ areas as well as the highest number of uniques, which was 11. Our morphological study showed a low number of specimens inhabiting nodules (surface/crevices), suggesting that specific kinorhynch species do not typically inhabit the nodules in addition to the surrounding sediment.

Keywords Meiofauna · Kinorhynchs · German contract area · Metabarcoding · Deep sea

This article is registered in ZooBank under http://zoobank.org/1B354AA1-DB24-41FA-9CF7-1D608C3705A2

This article is a contribution to the Topical Collection *Biodiversity in Abyssal Polymetallic Nodule Areas*

Communicated by S. Kaiser

✉ Nuria Sánchez
nurisanc@ucm.es

[1] Faculty of Biological Sciences, Department of Biodiversity, Ecology and Evolution, José Antonio Novais 12, Madrid 28040, Spain

[2] Senckenberg Am Meer, German Center for Marine Biodiversity Research, Südstrand 44, 26382 Wilhelmshaven, Germany

[3] Bundesanstalt für Geowissenschaften & Rohstoffe, Stilleweg 2, D-30655 Hannover, Germany

Introduction

Large, contiguous areas of the deep seafloor that are covered with polymetallic nodules are currently in the spotlight due to their potential strategic commercial value, as these nodules (potato-sized concretions) are formed by layers of iron and manganese hydroxides that contain economically interesting metals such as Cu, Ni, and Co (Halbach et al. 1975; Halbach and Fellerer 1980). Even though it is expected that nodules will be mined in the future in order to face the growing demand for these valuable metals (Clark et al. 2013), the biological diversity of such nodule fields is still poorly known, even for the mega- and macrofaunal realms (Amon et al. 2016; Glover et al. 2002; Janssen et al. 2015; Paterson et al. 1998; Smith et al. 2008a). The International Seabed Authority (ISA), which is in charge of regulating the exploration and exploitation activities in international waters, has developed a set of exploration regulations that require identification of all faunal components from nodule areas before exploitation can proceed. The development of a comprehensive environmental baseline is crucial in order to accurately predict and assess environmental impacts and to establish mining regulations that guarantee the effective preservation of the nodule field fauna (ISA 2013).

Regarding meiofauna, the smallest-sized benthic eukaryotic component (32–1000 μm), most studies have focused on the dominant groups, such as Nematoda and Copepoda (Markhaseva et al. 2017; Miljutin et al. 2011; Singh et al. 2016), whereas the groups of lower densities, the so-called "minor phyla," are commonly neglected. Kinorhyncha, a phylum of holobenthic, free-living, exclusively meiobenthic, marine ecdysozoans ranging in size from 100 to 1000 μm, also known as mud dragons, belongs to this pool of less common meiofaunal groups. Despite kinorhynchs having a world-wide distribution, from polar to equatorial latitudes and from the intertidal to the deep-sea floors, most described species have been recorded from relatively shallow waters while the deep-sea kinorhynch fauna is still largely unexplored (Cepeda et al. 2021; Neuhaus 2013, 2021; Yamasaki 2021). For deep-sea polymetallic nodule areas of the Clarion-Clipperton Fracture Zone (CCZ), in the north-eastern Pacific Ocean, one of the nodule fields of greatest commercial interest at an average depth of ca. 4200 m, Sánchez et al. (2019) described three new cyclorhagid species belonging to three different genera: *Cephalorhyncha polunga* Sánchez, Pardos & Martínez Arbizu, 2019, *Echinoderes shenlong* Sánchez, Pardos & Martínez Arbizu, 2019, and *Meristoderes taro* Sánchez, Pardos & Martínez Arbizu, 2019 (Sánchez et al. 2019). Moreover, the above-mentioned contribution also reported nine still undescribed species and the presence of five additional species (Sánchez et al. 2019).

The presence of deep-sea kinorhynchs has been reported in ecological studies, but identifications were generally limited to the phylum level (Carman et al. 2004; Neuhaus 2013; Shimanaga et al. 2000). More recently, research including identifications to the species level have increased, and up to 47 deep-sea species were described or reported in the last few years, pointing to a high deep-sea kinorhynch diversity (Adrianov and Maiorova 2015, 2016, 2018a, 2018b, 2019; Álvarez-Castillo et al. 2020; Cepeda et al. 2019a; Grzelak and Sørensen 2018, 2019; Grzelak et al. 2021; Neuhaus and Blasche 2006; Neuhaus and Sørensen 2013; Sánchez et al. 2014a, 2014b, 2019; Sørensen 2008; Sørensen et al. 2018, 2019; Sørensen and Grzelak 2018; Yamasaki et al. 2018a, 2018b, 2018c, 2019).

The aim of the present study is to provide a general overview of the kinorhynch biodiversity in the exploration contract areas of the CCZ, with a strong focus on the German contract area, as well as in the Peru Basin. Furthermore, three new *Echinoderes* species from the CCZ are described. A metabarcoding approach has been applied in addition to morphological examinations, to analyze the diversity and composition of CCZ meiofaunal communities (no metabarcoding samples were obtained in the Peru Basin).

Material and methods

Study areas

Meiofaunal communities were collected during ten research expeditions carried out in the CCZ and the Peru Basin (Fig. 1). In the BGR contract area (German Federal Institute for Geoscience and Natural Resources), kinorhynchs were obtained from 89 multicorer deployments and 205 cores, collected during eight cruises from 2010 to 2019: MANGAN 2010 (SO205; R/V Sonne) (Rühlemann et al. 2010), MANGAN 2013 (KM13; R/V Kilo Moana) (Rühlemann et al. 2014), MANGAN 2014 (KM14-08; R/V Kilo Moana) (Rühlemann et al. 2015), MANGAN 2016 (KM16; R/V Kilo Moana) (Rühlemann et al. 2017), FLUM 2015 (SO240; R/V Sonne) (Kuhn 2015), JPIO/CCZ (Joint Programming Initiative Healthy and Productive Seas and Oceans) (SO239; R/V Sonne) (Martínez Arbizu and Haeckel 2015), MANGAN 2018 (SO262; R/V Sonne) (Rühlemann et al. 2019), and MiningImpact 2 (SO268-2; R/V Sonne) (Haeckel and Linke 2021).

Kinorhynchs were also collected from the UKSR I contract area (UK Seabed Resources Ltd), which was sampled during the ABYSSLINE II cruise (TN319; R/V Thomas G. Thompson) (Smith and Shipboard Scientific Party 2013). Similarly, kinorhynchs were found in samples obtained from the GSR (Belgium, Global Sea Minerals Resources NV), Ifremer (France, Institut Français de Recherche pour L'exploitation De La Mer), and IOM (Inter Ocean Metal) contract areas as well as the ISA's APEI3 (Area of Particular

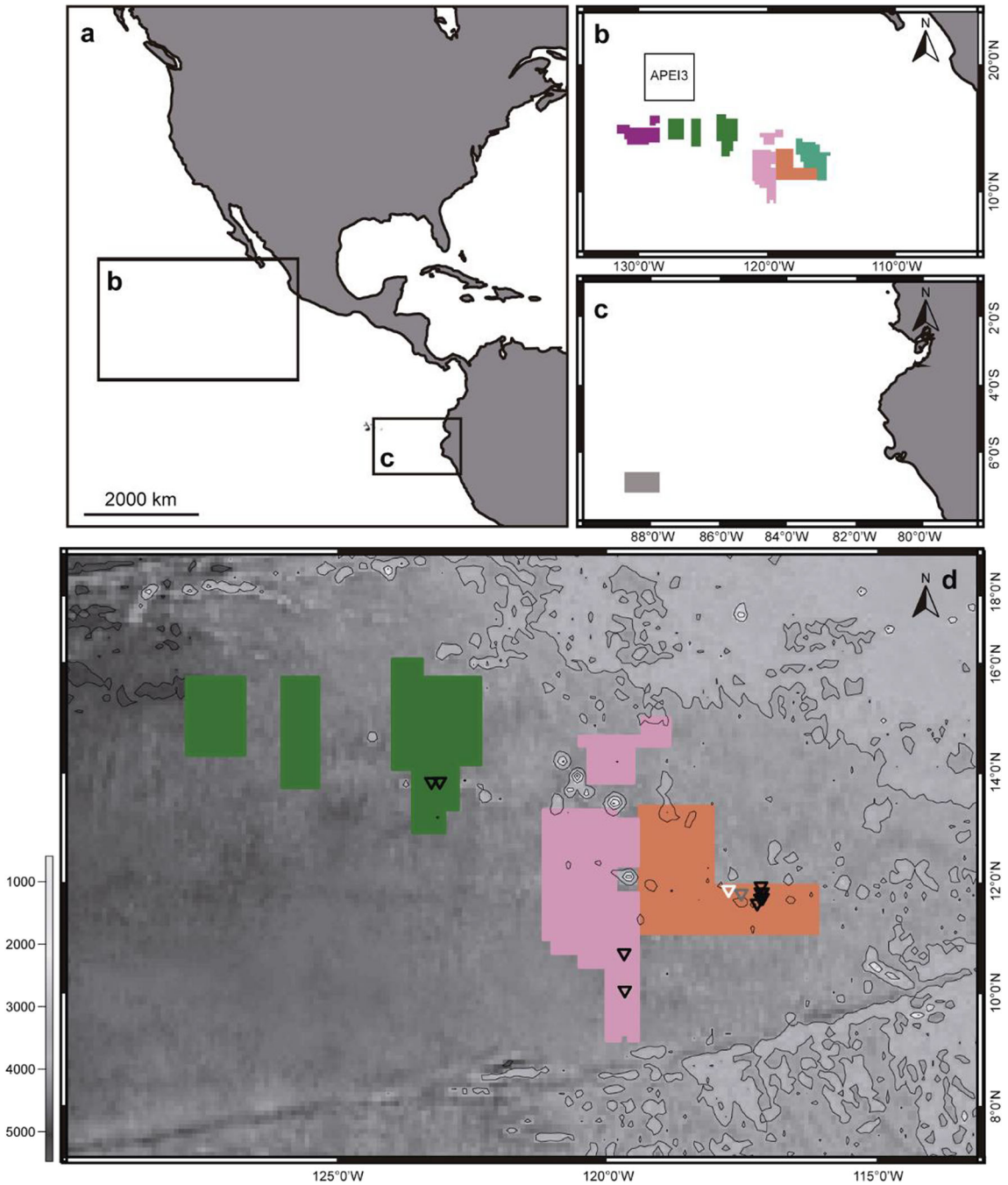

Fig. 1 **a** General map of the CCZ and Peru Basin locations; **b** CCZ, with the BGR contract area in orange; GSR area in dark green; Ifremer area in purple; IOM area in pink; UKSR I area in light green; **c** Peru Basin area in gray color; **d** stations and defined areas of the CCZ in which samples were obtained for metabarcoding studies; BGR contract area in orange; GSR area in dark green; IOM area in pink; triangles within the BGR, GSR and IOM areas define stations in which kinorhynch ASVs were detected. White triangles within the BGR area mark samples collected in the IRA1 area; gray triangles mark samples collected in the IRA Trial area, and black triangles mark samples collected in the BGR Reference and BGR Trial. The black/white gradient bar shows the water depth in meters under the medium sea level. Map created using the GEBCO_2014 Grid, version 20150318.

Environmental Interest number 3), which were sampled during the JPIO/CCZ (SO239; R/V Sonne). Finally, kinorhynchs were also collected in the Peru Basin during the JPIO/DISCOL cruise (SO242-1) (R/V Sonne), (Greinert 2015) specifically at the DEA Reference Area (DISCOL Experimental Area). Detailed information from each sampling site and cruise is provided in Online supplements and Table 1.

In order to analyze the kinorhynch community composition across different areas of the CCZ, six working areas from different contract areas were considered: BGR Reference

Table 1 Information on the cruises carried out in the CCZ and the Peru Basin in which samples were obtained for morphological studies

Cruise No.	Name of Cruise/Project	Ship	Year	Locality
SO205	MANGAN 2010	RV SONNE	2010	Equatorial NE Pacific Ocean, CCZ (Clarion-Clipperton Fracture-Zone), German Licence Area
KM14-08	MANGAN 2014	RV KILO MOANA	2014	Pacific Ocean, CCZ (Clarion-Clipperton Fracture-Zone), German Licence Area
SO240	FLUM 2015	RV SONNE	2015	Pacific Ocean, CCZ (Clarion-Clipperton Fracture-Zone), German Licence Area
SO239	JPIO/CCZ	RV SONNE	2015	Pacific Ocean, CCZ (Clarion-Clipperton Fracture-Zone), German, Belgian & French Claim
TN319	ABYSSLINE II	RV THOMAS G. THOMPSON	2015	Pacific Ocean, CCZ (Clarion-Clipperton Fracture-Zone), UK & Singapore Licence Area
SO242-1	JPIO/DISCOL	RV SONNE	2015	Pacific Ocean, CCZ (Clarion-Clipperton Fracture-Zone), DEA, Reference Area
KM16	MANGAN 2016	RV KILO MOANA	2016	Pacific Ocean, CCZ (Clarion-Clipperton Fracture-Zone), German Licence Area
SO262	MANGAN 2018	RV SONNE	2018	Equatorial NE Pacific Ocean, CCZ (Clarion-Clipperton Fracture-Zone), German Licence Area
SO268-2	MiningImpact 2	RV SONNE	2019	Equatorial NE Pacific Ocean, CCZ (Clarion-Clipperton Fracture-Zone), German & Belgian Licence Area

and BGR Trial area, Impact Reference Area 1 (IRA1) and IRA Trial area, GSR, and IOM. These areas show substantial differences in environmental characteristics such as sediment compositions, level of pigment and organic compounds, as well as nodule densities (e.g., Hauquier et al. 2019).

Sampling, processing, and kinorhynch identification

Samples were taken at abyssal depths using a multicorer with cores 9.4 cm of inner diameter, sampling a total surface area of 69 cm^2 by each core. See Online supplements for detailed information on each sampling site and the species found at each site. The upper 5 cm of the sediment were fixed on board with 4% buffered formalin for morphological analyses and DESS (Yoder et al. 2006) for genetic investigations. The colloidal silica polymer Levasil protocol was applied to extract metazoan meiofauna from the sediment (Neuhaus and Blasche 2006). Then, meiofauna was sorted and identified to the main taxonomic groups. When nodules were observed within cores, these were carefully removed on board and washed to obtain all sediment from their surfaces and crevices. This sediment was also fixed in 4% buffered formalin and meiofauna was subsequently sorted and identified as aforementioned. After sorting, a total of 779 kinorhynch specimens were picked and preserved in 70% or 96% ethanol.

Adult specimens were identified to species level using light microscopy (LM) or scanning electron microscopy (SEM). Specimens for LM were dehydrated through a graded series of glycerin and kept overnight in 100% glycerin. Then, the specimens were mounted in Fluoromount-G® on glass slides, studied, and photographed with an Olympus BX51® compound microscope with differential interference contrast (DIC) optics equipped with an Olympus DP70® camera. Specimens were measured using the cellSens® software. Kinorhynchs for SEM studies were dehydrated through a graded series of ethanol, and chemically dried using hexamethyldisilazane (HMDS) through a HMDS-ethanol series. Subsequently, specimens were examined with a JEOL Ltd. JSM-6335F field mission scanning electron microscope after mounted on SEM stubs and covered with gold (ICTS Centro Nacional de Microscopía Electrónica, Universidad Complutese de Madrid, Spain). Type and additional material of the new species were deposited at the Museum für Naturkunde Berlin (MfN), Germany (Table 2).

For DNA analyses, the meiofauna from 253 cores deriving from eight cruises between 2010 and 2019, including MANGAN 2010, MANGAN 2013, MANGAN 2014, JPIO/CCZ, MANGAN 2016, MANGAN 2018, MiningImpact 2, and the ABYSSLINE II cruises, were extracted using glass sterile filters (2.7 μm particle size). Samples from MANGAN 2013 are only included in the metabarcoding analyses but not for analyses of morphology, whereas no metabarcoding samples were obtained during the JPIO/DISCOL cruise in the Peru Basin. The filters (containing meiofauna) were dried using a speed-vacuum system for 1 h at 45 °C and stored in a sterile 1.5 Eppendorf mini-tube for DNA extraction.

DNA extraction, amplification, and high-throughput sequencing (HTS)

Genomic DNA from meiofauna communities was extracted using E.Z.N.A.® Mollusc DNA Kit (Omega BIO-TEK) following its protocol and the DNA was eluted in 100 μl of nuclease-free water for each library (sample). In order to amplify the V1 & V2 hypervariable regions of the 18S rRNA and

Table 2 Summary of data on stations and catalogue numbers for specimens of the new species

Project/cruise	Contract area	Station/Core	Collecting date	Latitude, Longitude	Depth (m)	Mounting	Type status, number and catalogue number for specimens of the new species
Mangan 2010 SO205	BGR	TV-MUC #13	28/4/10	11°19.16′ N, 119°18.433′ W	4325	LM	1♀ *Echinoderes delaordeni* sp. nov. ZMB 12427
Mangan 2010 SO205	BGR	TV-MUC #06	26/4/10	11°19.254′ N, 119°17.237′ W	4386	LM	1♀ paratype *Echinoderes sanctorum* sp. nov. ZMB 12439
Mangan 2010 SO205	BGR	TV-MUC #25	2/5/10	11°36.401′ N, 116°09.759′ W	4195	LM LM	1♀ paratype *Echinoderes sanctorum* sp. nov. ZMB 12440 1♀ paratype *Echinoderes zeppilliae* sp. nov. ZMB 12448
Mangan 2010 SO205	BGR	TV-MUC #51	8/5/10	11°57.265′ N, 116°59.545′ W	4118	LM	1♀ paratype *Echinoderes zeppilliae* sp. nov. ZMB 12449
Mangan 2010 SO205	BGR	TV-MUC #64	16/5/10	13°07.659′ N, 118°05.378′ W	4273	LM	1♀ paratype *Echinoderes sanctorum* sp. nov. ZMB 12441
Mangan 2014 KM14-08	BGR	MUC #93	23/5/14	11°16.217′ N, 117°14.315′ W	4189	LM LM	1♀ *Echinoderes delaordeni* sp. nov. ZMB 12428 1♀ holotype *Echinoderes sanctorum* sp. nov. ZMB 12438
Flum 2015 SO240	BGR	MUC #61	25/5/15	12°56.109′ N, 119°08.871′ W	4293	SEM	1♀ *Echinoderes sanctorum* sp. nov. ZMB 12446
Flum 2015 SO240	BGR	MUC #74	29/5/15	12°55.601′ N, 119°08.83′ W	4295	LM LM	1♀ holotype *Echinoderes delaordeni* sp. nov. ZMB 12419 1♀ paratype *Echinoderes sanctorum* sp. nov. ZMB 12442
JPIO/CCZ SO239	BGR	MUC #35	24/3/15	11°51.09′ N, 117°03.05′ W	4126	LM	1♀ paratype *Echinoderes delaordeni* sp. nov. ZMB 12420
JPIO/CCZ SO239	GSR	MUC #146	2015	13°50.74′ N, 123°15.10′ W	4511	SEM	1♀ *Echinoderes delaordeni* sp. nov. ZMB 12433
JPIO/CCZ SO239	Ifremer	MUC #154	2015	14°03.00′ N, 130°08.32′ W	4890	LM	1♀ paratype *Echinoderes sanctorum* sp. nov. ZMB 12443
Abyssline II TN319	UKSLR I	MC06	2015	12°34.743′ N, 116°41.221′ W	4234	LM	1♂ *Echinoderes delaordeni* sp. nov. ZMB 12432
Abyssline II TN319	UKSLR I	MC16	2015	12°25.196′ N, 116°37.474′ W	4137	SEM	1♀ *Echinoderes delaordeni* sp. nov. ZMB 12437
JPIO/DISCOL SO242-1	DEA, Ref. Site	44-MUC-10	2015	07°07.51′ S, 088°27.00′ W	4160	LM	1♀ paratype *Echinoderes delaordeni* sp. nov. ZMB 12423
JPIO/DISCOL SO242-1	DEA, Ref. Site	61-MUC-13	2015	07°04.28′ S, 088°27.79′ W	4151	LM	1♀ paratype *Echinoderes delaordeni* sp. nov. ZMB 12424
JPIO/DISCOL SO242-1	DEA, Ref. Site	64-MUC-15	7/8/15	07°04.42′ S, 088°27.85′ W	4153	LM	1♀ paratype *Echinoderes delaordeni* sp. nov. ZMB 12425
JPIO/DISCOL SO242-1	DEA, Ref. Site	90-MUC-23	2015	07°04.56′ S, 088°31.57′ W	4125	LM	1♀ paratype *Echinoderes delaordeni* sp. nov. ZMB 12426
JPIO/DISCOL SO242-1	DEA, Ref. Site	109-MUC-27	18/8/15	07°04.49′ S, 088°26.84′ W	4161	LM	1♀ *Echinoderes sanctorum* sp. nov. ZMB 12445
Mangan 2016 KM16	BGR	MUC #44	3/5/16	11°51.284′ N, 117°02.365′ W	4135	LM LM	1♀ paratype *Echinoderes delaordeni* sp. nov. ZMB 12421 1♀ holotype *Echinoderes zeppilliae* sp. nov. ZMB 12447
Mangan 2016 KM16	BGR	MUC #45	3/5/16	11°49.687′ N, 117°00.813′ W	4145	SEM LM LM	1♀ *Echinoderes delaordeni* sp. nov. ZMB 12434 1♀ *Echinoderes delaordeni* sp. nov. ZMB 12429 1♀ *Echinoderes delaordeni* sp. nov. ZMB 12430
Mangan 2016 KM16	BGR	MUC #49	4/5/16	11°50.513′ N, 117°00.523′ W	4121	SEM	1♂ *Echinoderes delaordeni* sp. nov. ZMB 12435
Mangan 2016 KM16	BGR	MUC #89	8/5/16	11°47.654′ N, 117°31.638′ W	4356	LM	1♀ paratype *Echinoderes zeppilliae* sp. nov. ZMB 12450
Mangan 2016 KM16	BGR	MUC #97	10/5/16	11°54.017′ N, 117°24.822′ W	4139	SEM	1♂ *Echinoderes delaordeni* sp. nov. ZMB 12436
Mangan 2016 KM16	BGR	MUC #104	11/5/16	11°53.795′ N, 117°27.905′ W	4202	LM	1♂ paratype *Echinoderes delaordeni* sp. nov. ZMB 12422
Mangan 2018 SO262	BGR	MUC #21	2018	11°55.692′ N, 117°00.954′ W	4090	LM	1♀ *Echinoderes sanctorum* sp. nov. ZMB 12444
Mangan 2018 SO262	BGR	MUC #33	2018	11°55.951′ N, 117°00.823′ W	4092	LM	1♀ paratype *Echinoderes zeppilliae* sp. nov. ZMB 12451
Mangan 2018 SO262	BGR	MUC #66	2018	11°51.468′ N, 117°01.351′ W	4127	LM	1♀ *Echinoderes delaordeni* sp. nov. ZMB 12431

attach the Illumina Unique Dual Nextera XT Indexes and compatible adapters, two PCRs were performed for each library. First PCR was conducted using SSU universal primers F04 and R22 (Blaxter et al. 1998) tagged by the first part of the Illumina adapters in total volume of 20 µl containing 10 µl of Phusion Green Hot Start II High-Fidelity PCR Master Mix (ThermoFisher), 0.5 µl of each primer (10 pmol/µl), 2 µl of genomic DNA, and 7 µl of molecular grade water. Cycler settings for the first PCR encompassed an initial denaturation step at 98 °C for 2 min, 25 cycles of denaturation at 98 °C for 15 s, annealing at 60 °C for 30 s, elongation at 72 °C for 30 s, and a final elongation at 72 °C for 2 min. A total of 5 µl of the first PCR products were purified using 2 µl of ExoSAP-IT PCR Product Cleanup Reagent (ThermoFisher). The second PCR was carried out to bind the Nextera XT Indexes and Illumina adapter overhang (according to Illumina 16S Metagenomic Sequencing Library Preparation guide (15044223Rev.B) using 7 µl of DNA template (purified first PCR product), 10 µl of Phusion Green Hot Start II High-Fidelity PCR Master Mix, 1 µl of molecular grade water, and 1 µl of each index primers from Nextera XT Indexes. The cycler setting consisted of an initial denaturation step at 98 °C for 2 min, 15 cycles of denaturation at 98 °C for 15 s, annealing and elongation at 72 °C for 35 s, and a final elongation at 72 °C for 2 min. The PCR products were run on a 1.5% agarose gel containing 1% GelRed to check the amplification and target fragment length. Considering the concentration of target products, 2 out of 10 µl of the tagged V1V2 amplicons were pooled and purified using AMPure XP Beads for PCR Purification (Beckman Coulter) in the amount of 60% of the total volume of the pooled libraries. The purified library was denatured and 15% PhiX control was added before performing test runs using MiSeq Reagent Nanokit v2 (150-cycles paired end), and final sequencing runs by MiSeq Reagent kit v3 (300-cycles paired end). In total, the prepared libraries of 253 stations were sequenced in 3 independent runs at the DZMB Metabarcoding lab in Wilhelmshaven (Germany) on an Illumina MiSeq platform.

Data processing and bioinformatics

The MiSeq Illumina next-generation sequencing (NGS) reads from each sequencing run were trimmed by both primers using BBMap tools (https://jgi.doe.gov/data-and-tools/software-tools/bbtools/bb-tools-user-guide/installation-guide/) applying kmer size of 15, number of kmer hits of 1, and allowed hamming distance of 1 (the script applied is "trimadaptV1V2.sh"). The DADA2 pipeline (Callahan et al. 2016), a Divisive Amplicon Ae-noising Algorithm for correcting Illumina errors, was used for denoising and filtering the reads by quality scores, detecting chimeras and de-replicating to high resolution amplicon sequence variants (ASVs) (applied commands are scripted as "SGN_dada2_batch_V1V2.r"). The ASVs from the three runs were merged using the script "mergingASVs.sh" and further processed by a costume script (SGN Metabarcoding pipeline so called "SGNpipeline_dada2_V1V2_march2020.sh") where all sequences shorter than 320 bp were eliminated. For taxonomic assignments, each ASV was blasted against the NCBI database (National Center for Biotechnology Information), and the 10 best blast hits were retrieved and pooled with the 18S reference library of the DNA barcode archive of the DZMB institute (German Center for Marine Biodiversity Research). This merged dataset was used as final blast database to assign the best and closest taxonomical assignment to each ASV. To evaluate the GenBank taxonomic assignments, a "Grade value" was designed and calculated as function of the blast query coverage multiple by 2, plus the percentage identity of each ASV divided into 3 ((qcov *2 + pident)/3), to have both parameters into account as a single value for each assignment. The ASV table containing taxonomical assignments, percentage identity, query coverage, GenBank accession number, *e* value, length of the read, and number of reads per library was analyzed using the "dada2pp" function (https://github.com/pmartinezarbizu/dada2pp) and the R package vegan v. 2.2-1 (Oksanen et al. 2015) to eliminate contaminations and to extract the kinorhynch ASVs from the final meiofauna community table. In addition, the kinorhynch ASVs were processed to produce graphics using R packages following the "postprocessing.r" script. All implemented scripts and kinorhynchs metabarcoding data used in this study are provided as Online supplements. Sequences from the kinorhynch ASVs were aligned using MAFFT v7.017 (Katoh et al. 2002) and a Bayesian tree was calculated from the alignment implying 5 million MCMC generations using BEAUti & The BEAST package (https://beast.community/beauti).

Statistical analysis

Differences in kinorhynch community structure between the contract areas of the CCZ and between the whole CCZ and the Peru Basin were addressed in terms of specimen, juvenile, and adult densities (number of individuals per 10 cm^2) using Kruskal–Wallis analysis (KW) available in the R v.6.3.1 software. Diversity and species composition comparisons were not analyzed and compared due to the strong sampling bias of our data in favor of the BGR contract area, which was clearly observed in the sample-based rarefaction curves for each area (R package vegan v. 2.2-1, Oksanen et al. 2015) (Online supplement). Tests of normality and homoscedasticity were also initially performed using the "shapiro.test," "ad.test," and "fligner.test" functions included in the R package nortest and in the R Base Package (R Core Team 2020). Morphological diversities were measured using the Shannon–Wiener diversity (H′, log-base *e*) and the Pielou (J′) indexes for evenness, using the "diversity" function included in the R

package vegan v. 2.2-1 (Oksanen et al. 2015). Pearson rank correlations were calculated to study the relationship among the kinorhynch species and between gender and juvenile density. Correlation analyses were implemented using the "cor" and "rcorr" functions included in the R package Hmisc v. 4.6-0 (Harrell Jr 2021).

Results

Taxonomic account

Class Cyclorhagida (Zelinka, 1896) Sørensen et al. 2015
Family Echinoderidae Carus, 1885
Genus *Echinoderes* Claparède, 1863
***Echinoderes delaordeni* sp. nov.**
http://zoobank.org/2FDFEF50-DC80-495F-8E20-66BEE7018E3A
(Figs. 2, 3, 4, and 5 and Tables 2, 3, and 4)

Synonymy Echinoderes sp. 1 (in Sánchez et al. 2019).

Material examined Holotype, adult female, collected on 29 May 2015 at the Clarion-Clipperton Fracture Zone (central-eastern Pacific Ocean), BGR license area: 12°55.601′ N 119°08.83′ W (Table 2) at 4295 m depth; mounted in Fluoromount G®, deposited at MfN under accession number: ZMB 12419. Paratypes, one adult male and six adult females, all of them collected at different stations than the holotype (Table 2), mounted in Fluoromount G® and stored at MfN under accession numbers: ZMB 12420-12426. Six additional specimens, one male and five females, mounted for LM deposited at the MfN as additional material (ZMB 12427-12432). Five additional specimens, two males and three females, mounted for SEM deposited at the MfN as additional material (ZMB 12433-12437).

Etymology The species name is dedicated to Mr. Javier de la Orden, husband of the first author, for many years of understanding, patience, and wholehearted support.

Diagnosis *Echinoderes* with spines in middorsal position on segments 4–8 and lateroventral position on segments 6–9, increasing in length posteriorly; tubes in ventrolateral position on segment 2, in lateroventral position on segment 5 and in laterodorsal position on segment 10; type 2 glandular cell outlets in subdorsal position on segments 2 and 4–9, bilateral symmetry not present in all referred segments; tergal extensions short, distally rounded.

Description The description refers to the most common patter; deviations from it are mentioned otherwise. See Table 3 for measurements and dimensions, and Table 4 for summary of spine, tube, nephridiopore, glandular cell outlet, female papilla, and sensory spot locations.

Head with retractable mouth cone and introvert (Fig. 3a–c). Only one of the examined specimens had the head everted, but oral styles and scalids tend to collapse when mounted for LM, hence only some details on the morphology and arrangement of these structures are provided. Inner oral styles of ring − 01 of the mouth cone composed of two jointed subunits: a narrowed, rectangular, superficially fringed basis and an elongated, hook-like distal structure. External part of mouth cone (ring 00) with nine outer oral styles, alternating in size between slightly longer and slightly shorter ones: five long styles, anterior to the odd-numbered introvert sectors; four slightly shorter ones, anterior to the even-numbered ones, except in the middorsal section 6 where a style is missing. Outer oral styles also with two jointed subunits: a widened, rectangular, apparently smooth basis and a syringe-like, poorly sclerotized, distal end-piece.

Ring 01 of introvert with ten primary spinoscalids, with a long basal sheath and a distal end-piece (Fig. 3c). Remaining rings with regular-sized scalids (Fig. 3c), similar to the primary spinoscalids but smaller and more sclerotized.

Neck with sixteen elongated, trapezoidal placids, wider at base, approximately three to four times longer than wide, with a distinct joint between the neck and segment 1 (Fig. 3a, b, d); midventral one widest (ca. 17–18 μm wide at base) (Fig. 3b), remaining ones narrower ((ca. 8–10 μm wide at base) (Fig. 3a, b, d). Placids closely situated at base, distally separated by cuticular folds (Fig. 3a, b, d). A ring of six short, hairy trichoscalids associated with the placids of the neck present, attached to small, three-lobed trichoscalid plates (Fig. 3c).

Trunk with eleven segments (Figs. 2a–d; 3a, b; and 5a). Segments 1–2 as closed cuticular rings, remaining ones with one tergal and two sternal cuticular plates (Figs. 2a–d and 3a, b, e). Tergal plates of anterior segments slightly bulging middorsally, posterior ones more flattened, giving the animal a tapering outline in lateral view (Fig. 5a). Sternal plates reach their maximum width at segment 7, progressively tapering toward the last trunk segments; sternal plates relatively narrow compared to the total trunk length, giving the animal a slender appearance. Cuticular hairs acicular, long, bracteate, emerging from rounded to oval-shaped perforation sites (Figs. 3e; 4a, b; and 5a–h). Cuticular hairs distributed in 8–9 straight, transverse rows on segment 1; in 6–8 straight, transverse rows from paradorsal to ventrolateral region on segments 2–10, becoming wavy at the ventrolateral position; absent in laterodorsal position on segments 3–10 and on segment 11 (Fig. 2a–d). Primary pectinate fringes straight, serrated, showing a characteristic fringe alternating a longer tip and a series of 2-3 shorter tips, giving it a frayed appearance (Fig. 5b–d). Secondary pectinate fringes absent.

Segment 1 without spines and tubes (Figs. 2a, b; 3d, e; and 5a, c). Unpaired type 1 glandular cell outlet in middorsal

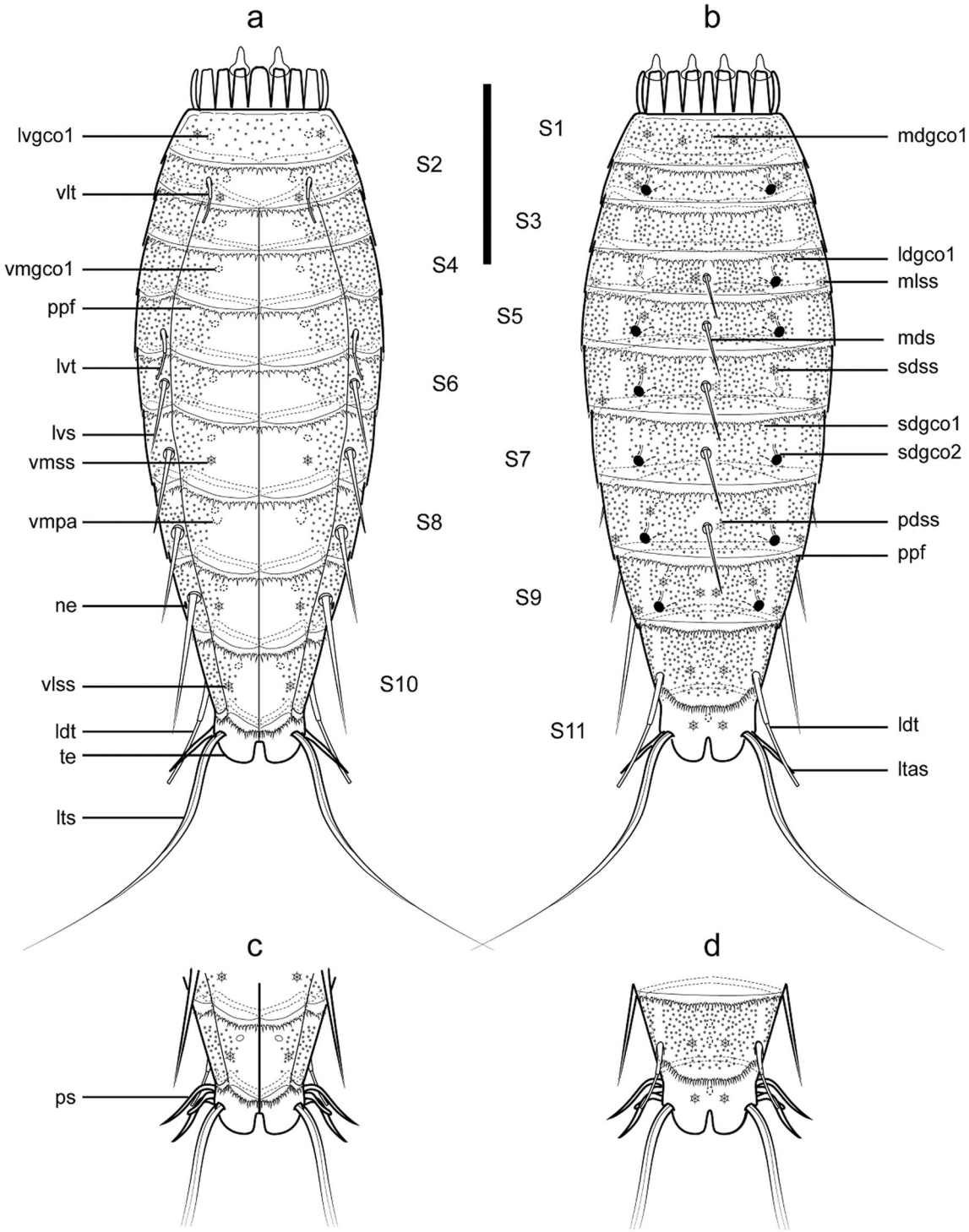

Fig. 2 Line art illustrations of *Echinoderes delaordeni* sp. nov. **a** Female, ventral view; **b** female, dorsal view; **c** male, ventral view of segments 10–11; **d** male, dorsal view of segments 10–11. Scale bar: 100 µm. *ldgco1* laterodorsal type 1 glandular cell outlet, *ldt* laterodorsal tube, *ltas* lateral terminal accessory spine, *lts* lateral terminal spine, *l-vgco1* lateroventral type 1 glandular cell outlet, *lvs* lateroventral spine, *lvt* lateroventral tube, *mdgco1* middorsal type 1 glandular cell outlet, *mds* middorsal spine, *mlss* midlateral sensory spot, *ne* nephridiopore, *pdss* paradorsal sensory spot, *ppf* primary pectinate fringe, *ps* penile spine, *sdgco1* subdorsal type 1 glandular cell outlet, *S1–S11* trunk segment, *sdgco2* subdorsal type 2 glandular cell outlet, *sdss* subdorsal sensory spot, *te* tergal extension, *vlss* ventrolateral sensory spot, *vlt* ventrolateral tube, *vmgco1* ventromedial type 1 glandular cell outlet, *vmpa* ventromedial female papilla, *vmss* ventromedial sensory spot

position, and paired type 1 glandular cell outlets in lateroventral position (Figs. 2a, b and 3d). Paired sensory spots in subdorsal, laterodorsal and sublateral positions, located at the anterior half of the segment, the latter pair situated

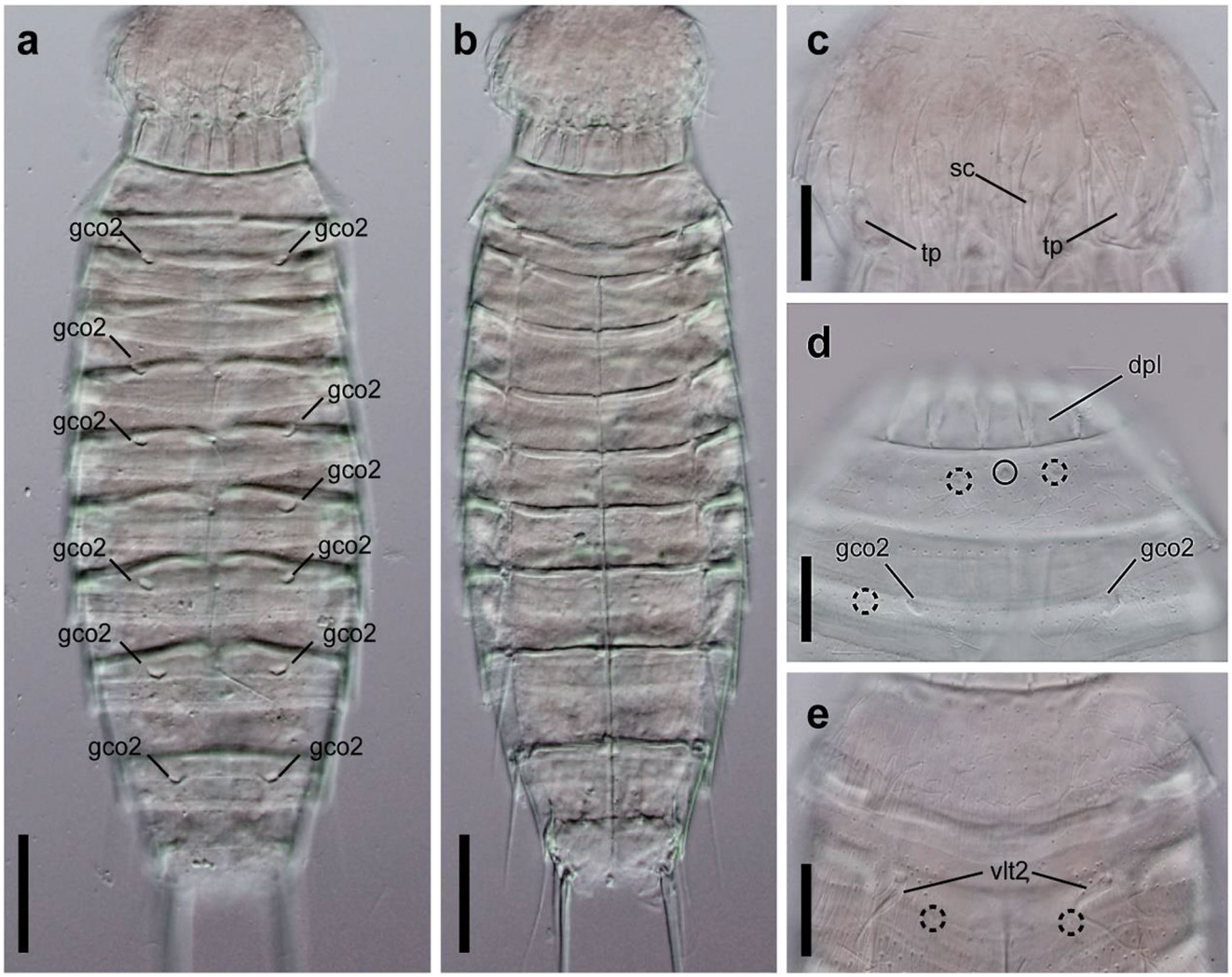

Fig. 3 DIC photographs of *Echinoderes delaordeni* sp. nov. **a**–**c**, **e** Paratypic female. **d** Holotypic female. **a** Dorsal overview; **b** ventral overview; **c** dorsal view of introvert; **d** dorsal view of neck and segments 1–2; **e** ventral view of segments 1–2. Dashed circles indicate sensory spots, and closed circles indicate type 1 glandular cell outlets; digits after abbreviations indicate the corresponding segment. Scale bars: **a**–**b** 50 µm; **c**–**e** 25 µm. *dpl* dorsal placid, *gco2* type 2 glandular cell outlet, *sc* regular-sized scalid, *tp* trichoscalid plate, *vlt* ventrolateral tube

next to the lateroventral type 1 glandular cell outlets (Figs. 2a, b and 3d). Sensory spots on this and following segments are extremely small, difficult to visualize under LM, with a single ring of micropapillae surrounding a tiny pore (Fig. 5b).

Segment 2 with tubes in ventrolateral position (Figs. 2a and 3e). Unpaired type 1 glandular cell outlet in middorsal position and paired ones in ventromedial position (Fig. 2a, b). Pair type 2 glandular cell outlets in subdorsal position, with a large and well-developed opening (Figs. 2b; 3a, d; and 5a–c). Two pairs of sensory spots in laterodorsal position, lateral to the subdorsal type 2 glandular cell outlets (one specimen with one sensory spot on either side of the glandular outlet), and one pair in ventromedial position (Figs. 2a, b; 3d, e; and 5b).

Segment 3 without spines and tubes (Figs. 2a, b and 5a–c). Unpaired type 1 glandular cell outlet in middorsal position, and paired ones in ventromedial position (Fig. 2a, b). Two specimens apparently with a subdorsal pair of sensory spots.

Segment 4 with a middorsal spine not exceeding half of the plate of the following segment (Figs. 2b; 4a; and 5c). Paired type 1 glandular cell outlets in laterodorsal and ventromedial positions (Fig. 2a, b). Paired type 2 glandular cell outlets in subdorsal position, with a large and well-developed opening (Figs. 2b, 3a, 4a, and 5c); deviations from the bilateral pattern were observed in some specimens, with an unpaired type 2 glandular cell outlet situated on a single side of the animal (from segment 4 to 7), on the right side in nine specimens (including the holotype) and on the left side in two specimens (Figs. 3a and 4a). Sensory spots only undoubtedly observed in midlateral position in four specimens (Figs. 2b and 5b); and unpaired paradorsal sensory spots in twelve specimens. Midlateral sensory spots especially small, next to the free flap region.

Segment 5 with a middorsal spine, not exceeding half of the plate of the following segment, and paired tubes in

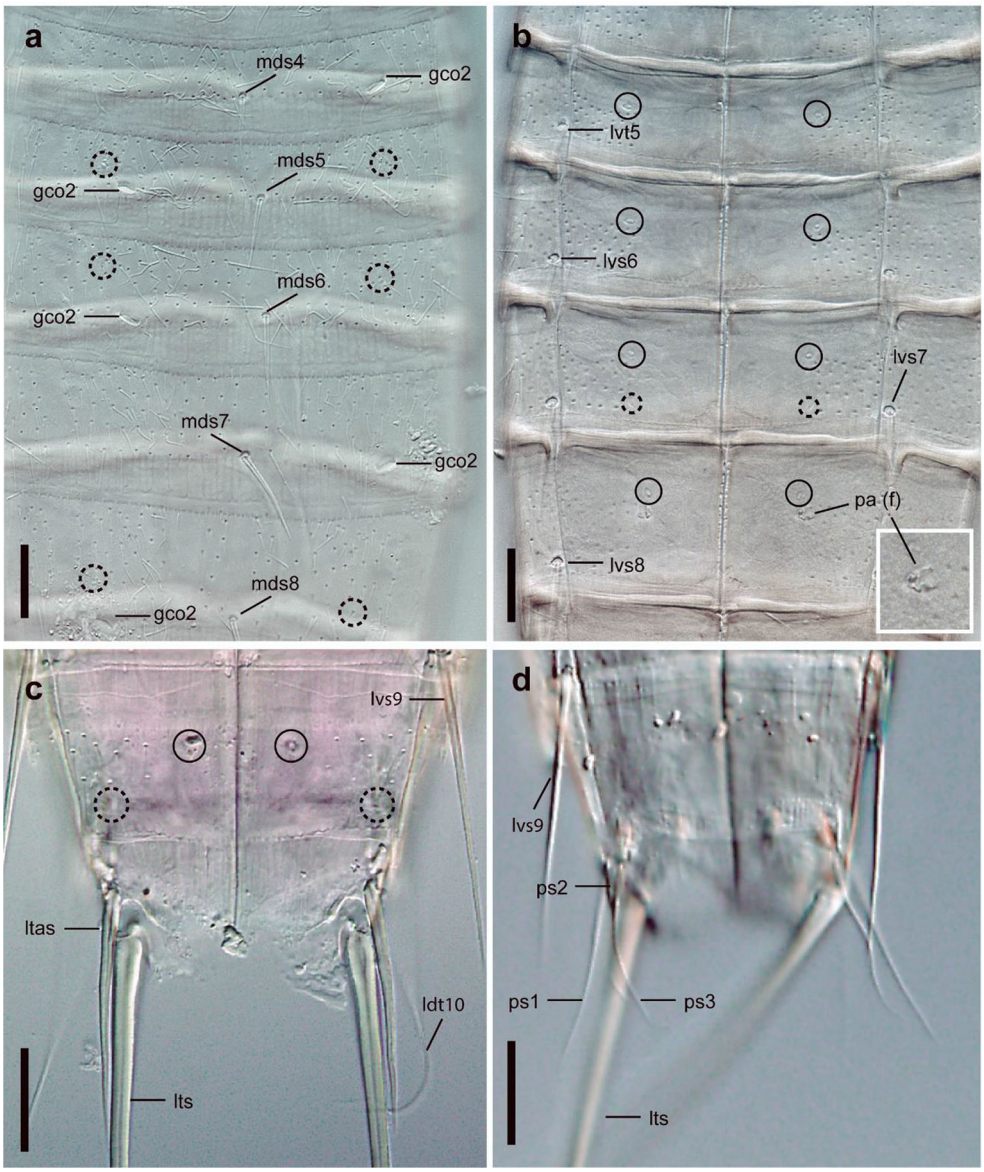

Fig. 4 DIC photographs of *Echinoderes delaordeni* sp. nov. **a**–**c** Holotypic female. **d** Paratypic male. **a** Dorsal view of segments 4–8; **b** ventral view of segments 5–8 (inset details the female papilla); **c** ventral view of segments 10–11; **d** ventral view of segments 10–11. Dashed circles indicate sensory spots, and closed circles indicate type 1 glandular cell outlets; digits after abbreviations indicate the corresponding segment (or the corresponding pair of penile spines in the case of these structures). Scale bars: **a**–**d** 25 µm. *f* female sexually dimorphic condition of a character, *gco2* type 2 glandular cell outlets, *ldt* laterodorsal tube, *ltas* lateral terminal accessory spine, *lts* lateral terminal spine, *lvs* lateroventral spine, *lvt* lateroventral tube, *mds* middorsal spine, *pa* female papilla, *ps* penile spine

lateroventral position (Figs. 2a, b; 3a; 4a, b; and 5c). Paired type 1 glandular cell outlets in subdorsal and ventromedial positions (Figs. 2a, b and 4b). Paired type 2 glandular cell outlets in subdorsal position (Figs. 2b; 3a; 4a; and 5a, c); although an unpaired outlet was observed at the right side in one specimen and at the left side in four specimens (including the holotype) (Fig. 4a). Paired sensory spots in subdorsal position, located anterior to the type 2 glandular cell outlets (Figs. 2b and 4a); at least one specimen with an unpaired subdorsal sensory spot at the left side.

Segment 6 with a middorsal spine, not exceeding half of the plate of the following segment, and paired spines in lateroventral position (Figs. 2a, b and 4a, b). Paired type 1 glandular cell outlets in laterodorsal and ventromedial positions (Figs. 2a, b and 4b). Paired type 2 glandular cell outlets in subdorsal position (Figs. 2b; 3a; 4a; and 5a); although an unpaired outlet was observed on the right side in three specimens and on the left side in eleven specimens (including the holotype) (Figs. 3a and 4a). Paired sensory spots in subdorsal position, located anterior to the type 2 glandular cell outlets (Figs. 2b and 4a); in laterodorsal position, lateral to the hairless areas (fourteen specimens, two males and twelve females). Laterodorsal sensory spots on this and on following segments especially small and difficult to observe, next to the free flap region. Unpaired paradorsal sensory spots seem to be present in at least nine specimens. Deviations from the common pattern of sensory spot distribution were also observed in the ventral side, with ventromedial sensory spots present in one female.

Segment 7 with a middorsal spine, reaching half of the tergal plate of the following segment, and paired spines in lateroventral position (Figs. 2a, b; 4a, b; and 5a, d, f). Paired

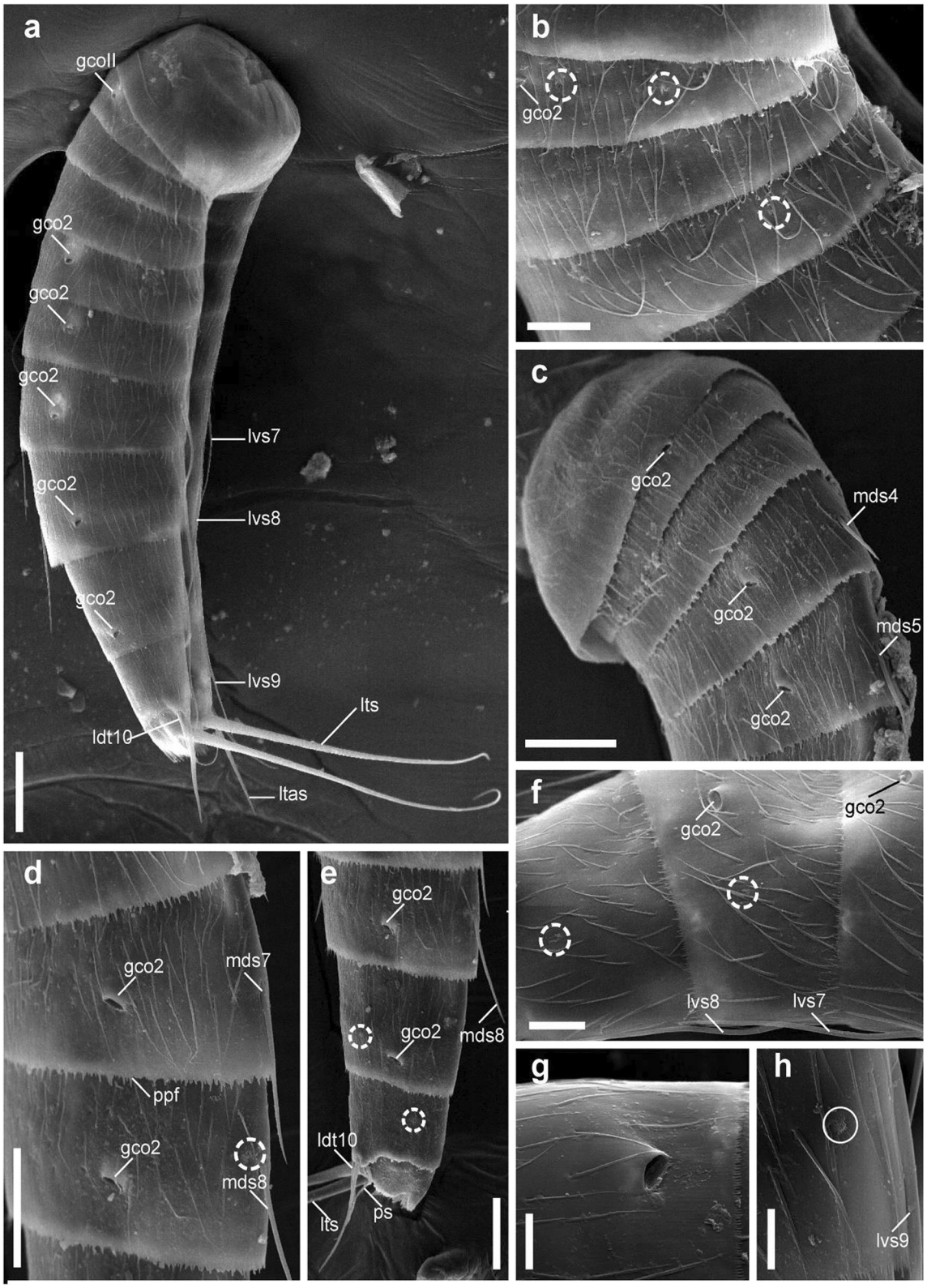

Fig. 5 SEM micrographs of *Echinoderes delaordeni* sp. nov. **a**, **g**–**h** Female, additional material; **b**, **f** female, additional material; **c**–**e** male, additional material. **a** Dorsolateral overview; **b** right half view of segments 2–4; **c** left half view of segments 1–5; **d** left half view of segments 7–8; **e** left half view of segments 8–11; **f** right half view of segments 7–9; **g** detail of the type 2 glandular cell outlet of segment 9; **h** detail of the nephridiopore, left side of segment 9. Dashed circles indicate sensory spots. Closed circle indicates the nephridiopore. Digits after abbreviations indicate the corresponding segment. Scale bar: **a** 30 μm; **b**, **f**, 10 μm; **c**–**e** 20 μm; **g**–**h** 5 μm. *gco2* type 2 glandular cell outlet, *ldt* laterodorsal tube, *ltas* lateral terminal accessory spine, *lts* lateral terminal spine, *lvs* lateroventral spine, *mds* middorsal spine, *ppf* primary pectinate fringe, *ps* penile spine

Table 3 Measurements (μm) and proportions of *Echinoderes delaordeni* sp. nov. Numbers in the first column indicate the corresponding segment. *LD* laterodorsal tube, *LTAS* lateral terminal accessory spine, *LTS* lateral terminal spine, *LV* lateroventral spine/tube, *MD* middorsal spine, *MSW* maximum sternal width, measured on segment 7, *n* number of measured specimens, *S* segment length, *SD* standard deviation, *SW* standard width, measured on segment 10; *TL* total trunk length, *VL* ventrolateral tube

	Holotype	*n*	♂	Mean ♀	Mean	Range	SD
TL	331	1♂/9♀	313	332	330	302–371	18.84
MSW 7	92	1♂/7♀	81	86	85	81–93	4.28
MSW/TL	28%	1♂/7♀	26%	26%	26%	23–28%	1.8
SW10	71	1♂/8♀	65	67	67	63–72	3.13
S1	41	1♂/6♀	38	36	36	30–41	3.99
S2	26	1♂/6♀	30	29	29	26–34	2.82
S3	34	1♂/7♀	30	32	32	24–38	4.48
S4	38	1♂/7♀	33	36	36	32–38	2.26
S5	41	1♂/7♀	34	38	38	34–44	3.64
S6	46	1♂/7♀	39	45	44	39–49	3.64
S7	47	1♂/7♀	41	46	46	41–51	3.12
S8	54	1♂/7♀	47	54	53	47–61	4.20
S9	57	1♂/7♀	55	57	57	54–62	2.84
S10	49	1♂/7♀	47	48	48	42–55	4.13
S11	37	1♂/6♀	27	29	29	26–37	3.97
MD4	19	1♂/6♀	25	21	21	17–25	3.57
MD5	19	1♂/6♀	30	24	25	20–30	4.53
MD6	19	1♂/6♀	32	27	27	19–33	5.11
MD7	25	1♂/6♀	37	31	32	23–41	7.75
MD8	28	1♂/6♀	44	36	37	28–44	6.51
VL2	–	0♂/3♀	–	24	24	11–46	19.29
LV5	24	1♂/6♀	16	25	23	16–31	5.35
LV6	25	1♂/8♀	31	29	29	24–34	3.12
LV7	32	1♂/5♀	45	38	39	32–45	4.91
LV8	39	1♂/8♀	51	47	48	39–54	5.27
LV9	46	1♂/8♀	70	57	58	46–70	6.30
LD10	51	1♂/8♀	52	55	54	39 –73	9.10
LTS	158	1♂/8♀	184	163	165	134–184	14.92
LTAS	41	8♀	–	50	49	41–53	3.75
LTS/TL	48%	1♂/8♀	59%	49%	50%	41–59%	5.75
LTAS/TL	12%	8♀	–	15%	15%	12–16%	1.42
LTAS/LTS	26%	8♀	–	30%	30%	26–37%	3.13

type 1 glandular cell outlets in subdorsal and ventromedial positions (Figs. 2a, b and 4b). Paired type 2 glandular cell outlets in subdorsal position (Figs. 2b; 3a; 4a; and 5a, d, f); although an unpaired outlet was observed on the right side in four specimens (including the holotype) and on the left side in two specimens (Fig. 4a). Paired sensory spots in ventromedial position (Figs. 2a and 4b).

Segment 8 similar to segment 7 in the arrangement of spines and glandular cell outlets (Figs. 2a, b; 3a; 4a, b; and 5a, d–f). Paired subdorsal and laterodorsal sensory spots; the latter pair situated lateral to the hairless areas; unpaired sensory spots in paradorsal position could be confirmed in nine specimens (Figs. 2b; 4a; and 5d, f). Female papillae of undetermined morphology in ventromedial position, close to the type 1 glandular cell outlets (Figs. 2a and 4b), with an opening similar to a type 1 glandular cell outlet but bigger, and a crescentic, subcuticular structure (see inset of Fig. 4b). Deviations from the common pattern of sensory spot distribution were observed in six specimens, two females without the subdorsal pair; the laterodorsal sensory spots could not be confirmed in three females and three males.

Segment 9 with paired lateroventral spines exceeding the tergal tips (Figs. 2a; 4c, d; and 5a). Paired type 1 glandular cell outlets in subdorsal and ventromedial positions (Figs. 2a, b). Paired type 2 glandular cell outlets in subdorsal position (Figs. 2b; 3a; and 5a, e, g). Sensory spots in paradorsal, subdorsal, laterodorsal, and ventrolateral positions (Fig. 2a, b), with the laterodorsal pair located lateral to the hairless cuticular areas (Fig. 5f). The laterodorsal sensory spots could not be confirmed in one female and two males. Nephridiopore as a small

Table 4 Summary of relevant cuticular characters and positions of *Echinoderes delaordeni* sp. nov. The most common pattern is provided. *LA* lateral accessory, *LD* laterodorsal, *LV* lateroventral, *MD* middorsal, *ML* midlateral, *PD* paradorsal, *PV* paraventral, *SD* subdorsal, *SL* sublateral, *VL* ventrolateral, *VM* ventromedial, *ac* acicular spine, *gco1/2* type 1/2 glandular cell outlet, *ltas* lateral terminal accessory spine, *lts* lateral terminal spine, *pa* papilla, *ps* penile spine, *si* sieve plate, *ss* sensory spot, *t* tube, ♂ male condition of sexually dimorphic characters, ♀ female condition of sexually dimorphic characters, * unpaired feature

Position segment	MD	PD	SD	LD	ML	SL	LA	LV	VL	VM	PV
1	gco1		ss	ss		ss		gco1			
2	gco1		gco2	ss,ss					t	gco1,ss	
3	gco1									gco1	
4	ac	ss	gco2*	gco1	ss					gco1	
5	ac		ss,gco2,gco1					t		gco1	
6	ac		ss,gco2*	gco1,ss				ac		gco1	
7	ac		gco2,gco1					ac		gco1,ss	
8	ac	ss	ss,gco2,gco1	ss				ac		gco1,pa(♀)	
9		ss	ss,gco2,gco1	ss			si	ac	ss	gco1	
10	gco1,gco1		ss	t					ss		gco1
11	gco1		ss		3x ps(♂)		ltas(♀)	lts			

opening surrounded by short papillae present in lateral accessory position (Fig. 5h).

Segment 10 with long laterodorsal tubes, almost reaching the tip of the lateral terminal accessory spines in females and surpassing the penile spines in males (Figs. 2a–d and 5a, e). Two unpaired type 1 glandular cell outlets in middorsal position, and paired type 1 glandular cell outlets in paraventral position (Figs. 2a–d and 4c). Paired sensory spots in subdorsal and ventrolateral positions (Figs. 2a–d; 4c; and 5e).

Segment 11 with lateral terminal spines long and slender, distally pointed, showing a hollow central cavity (Figs. 2a–d; 4c, d; and 5a, e). Females with paired, wide, and elongate lateral terminal accessory spines, about three to four times shorter than lateral terminal spines (Figs. 2a, b; 4c; and 5a). Males with three pairs of penile spines, arising laterally under the pectinate fringe of the preceding segment; ventral and dorsal penile spines (ps1 and ps3) filiform, midlateral one (ps2) shorter and broader (Figs. 2c, d; 4d; and 5e). Tergal and sternal extensions short, distally rounded (Figs. 2a–d and 5e). Unpaired type 1 glandular cell outlet in middorsal position (Fig. 2b, d). Paired sensory spots in subdorsal position (Fig. 2b, d).

Echinoderes sanctorum sp. nov.

http://zoobank.org/453970DD-C42A-42CE-A961-08D650368A65
(Figs. 6, 7 and 8 and Tables 2, 5 and 6)

***Synonymy Echinoderes* sp. 2 (in Sánchez et al. 2019).**

Material examined Holotype, adult female, collected on 23 May 2014 at the Clarion-Clipperton Fracture Zone (central-eastern Pacific Ocean), BGR license area: 11°16.217′ N, 117°14.315′ W (Table 2) at 4189 m depth; mounted in Fluoromount G®, deposited at MfN under accession number: ZMB 12438. Paratypes, five adult females, all of them collected at different stations than the holotype (see Table 2), mounted in Fluoromount G® and stored at MfN under accession numbers: ZMB 12439-12443. Two additional females mounted for LM deposited at the MfN as additional material (ZMB 12444-12445). One additional female mounted for SEM deposited at the MfN as additional material (ZMB 12446).

Etymology The species name refers to the mother's family name of the first author, *Santos* (Latin *sanctus*), taken here as a collective name (Latin *sanctorum*).

Diagnosis *Echinoderes* with spines in middorsal position on segments 4–8 and lateroventral position on segments 6–9, increasing in length posteriorly; tubes in ventrolateral position on segment 2, in lateroventral position on segment 5 and in laterodorsal position on segment 10; bilateral type 2 glandular cell outlets in subdorsal position on segment 1 and in laterodorsal position on segments 2-9; tergal extensions short, distally rounded.

Description See Table 5 for measurements and dimensions, and Table 6 for summary of spine, tube, nephridiopore, glandular cell outlet, female papilla, and sensory spot locations.

Head with retractable mouth cone and introvert. None of the examined specimens had the introvert everted, hence details on oral style and scalid morphology and arrangement cannot be provided.

Neck with sixteen elongated, trapezoidal placids, wider at base, approximately two to three times longer than wide, with a distinct joint between the neck and segment 1 (Figs. 6a, b

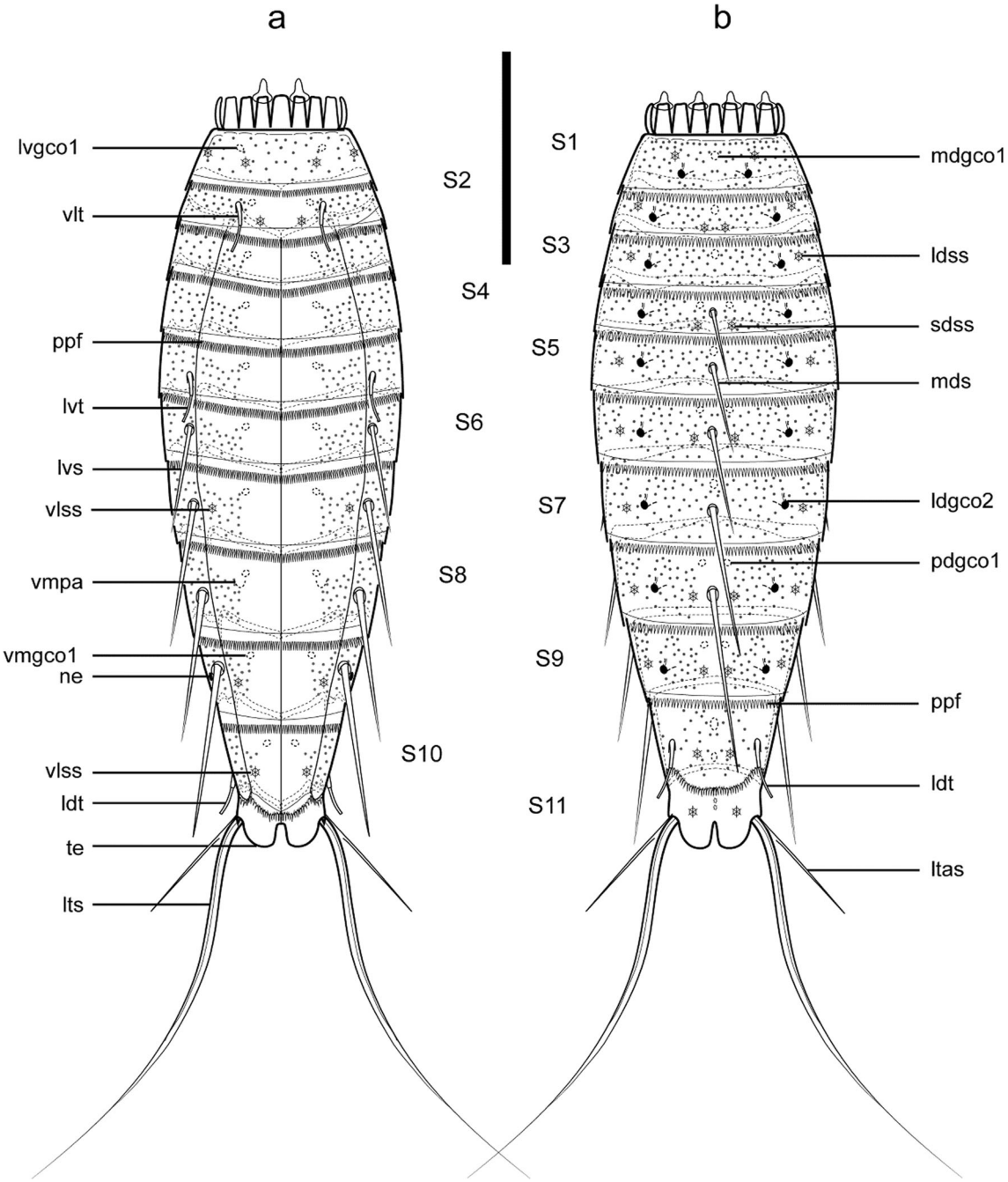

Fig. 6 Line art illustrations of *Echinoderes sanctorum* sp. nov. **a** Female, ventral view; **b** female, dorsal view. Scale bar: 100 µm. *ldgco2* laterodorsal type 2 glandular cell outlet, *ldss* laterodorsal sensory spot, *ldt* laterodorsal tube, *ltas* lateral terminal accessory spine, *lts* lateral terminal spine, *l-vgco1* lateroventral type 1 glandular cell outlet, *lvs* lateroventral spine, *lvt* lateroventral tube, *mdgco1* middorsal type 1 glandular cell outlet, *mds* middorsal spine, *ne* nephridiopore, *pdgco1* paradorsal type 1 glandular cell outlet, *ppf* primary pectinate fringe, *S1–S11* trunk segment, *sdss* subdorsal sensory spot, *te* tergal extension, *vlss* ventrolateral sensory spot, *vlt* ventrolateral tube, *vmgco1* ventromedial type 1 glandular cell outlet, *vmpa* ventromedial papilla

and 7a–d); midventral one widest (ca. 17–18 µm wide at base), remaining ones narrower (ca. 8–10 µm wide at base) (Figs. 6a, b and 7a–d). Placids closely situated at base, distally separated by cuticular folds. A ring of six short, hairy trichoscalids associated with the placids of the neck is present, attached to small, three-lobed trichoscalid plates (Fig. 6a, b).

Trunk with eleven segments. Segments 1–2 as closed cuticular rings, remaining ones with one tergal and two sternal cuticular plates (Figs. 6a, b; 7a–h; and 8a, b). Tergal plates of anterior segments slightly bulging middorsally, posterior ones more flattened, giving the animal a tapering outline in lateral view (Fig. 8a). Sternal plates reaching their

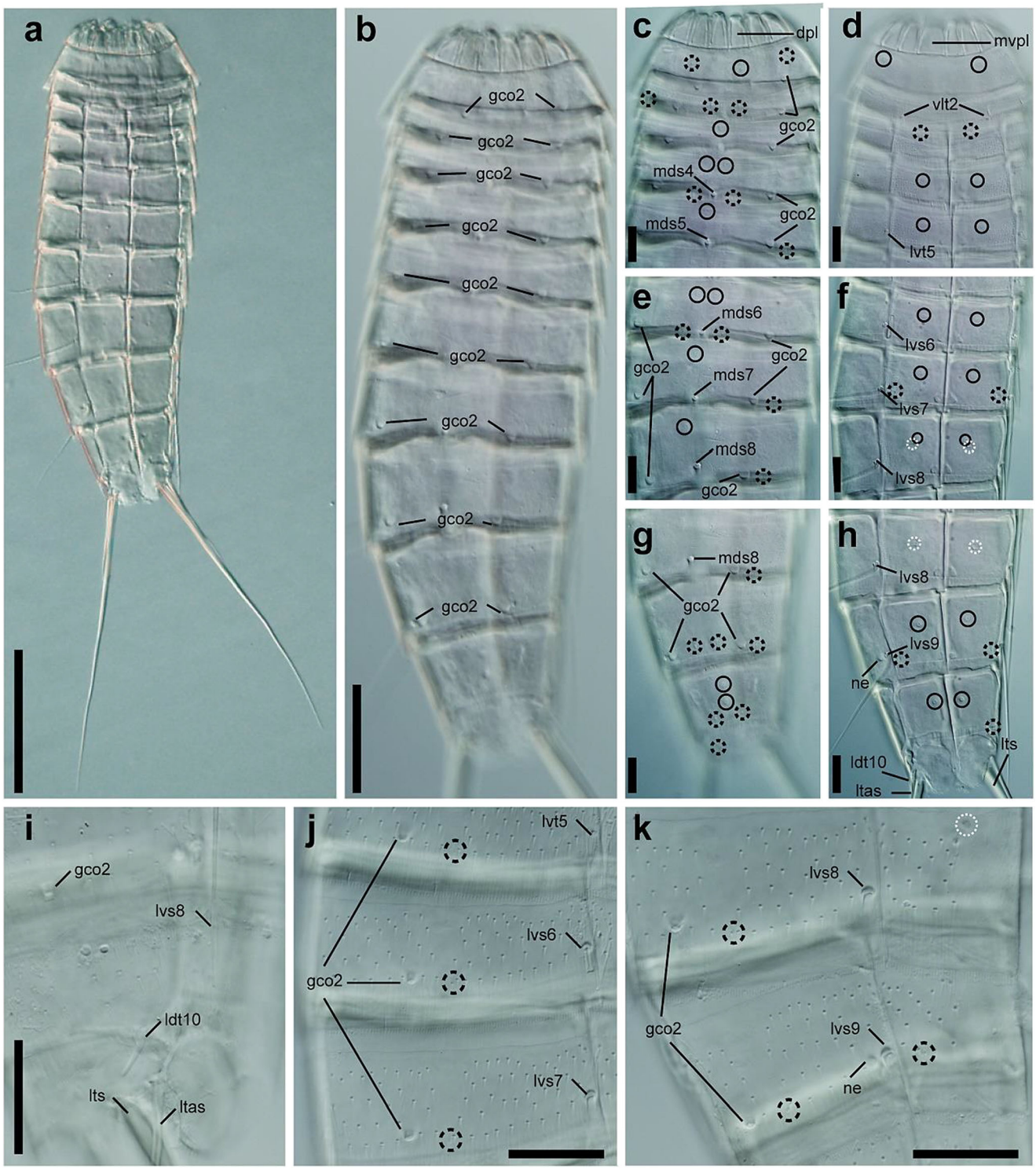

Fig. 7 DIC photographs of *Echinoderes sanctorum* sp. nov. **a**–**h** Holotypic female. **i**–**k** Paratypic female. **a** Ventral overview; **b** dorsal overview; **c** dorsal view of neck and segments 1–5; **d** ventral and lateral views of neck and segments 1–5; **e** dorsal view of segments 6–8; **f** ventral and lateral views of segments 6–8; **g** dorsal view of segments 8–11; **h** ventral and lateral views of segments 8–11; **i** right lateral view of segments 9–11; **j** lateral view of right half of segments 5–7, from subdorsal to lateroventral positions; **k** right lateral view of segments 8–9, from laterodorsal to paraventral positions. Dashed black circles indicate sensory spots. Dashed white circles indicate female papillae. Closed circles indicate type 1 glandular cell outlets. Digits after abbreviations indicate the corresponding segment. Scale bar: **a** 100 μm; **b** 50 μm; **c**–**k**, 25 μm. *dpl* dorsal placid, *gco2* type 2 glandular cell outlet, *ldt* laterodorsal tube, *ltas* lateral terminal accessory spine, *lts* lateral terminal spine, *lvs* lateroventral spine, *lvt* lateroventral tube, *mds* middorsal spine, *mvpl* midventral placid, *ne* nephridiopore, *vlt* ventrolateral tube

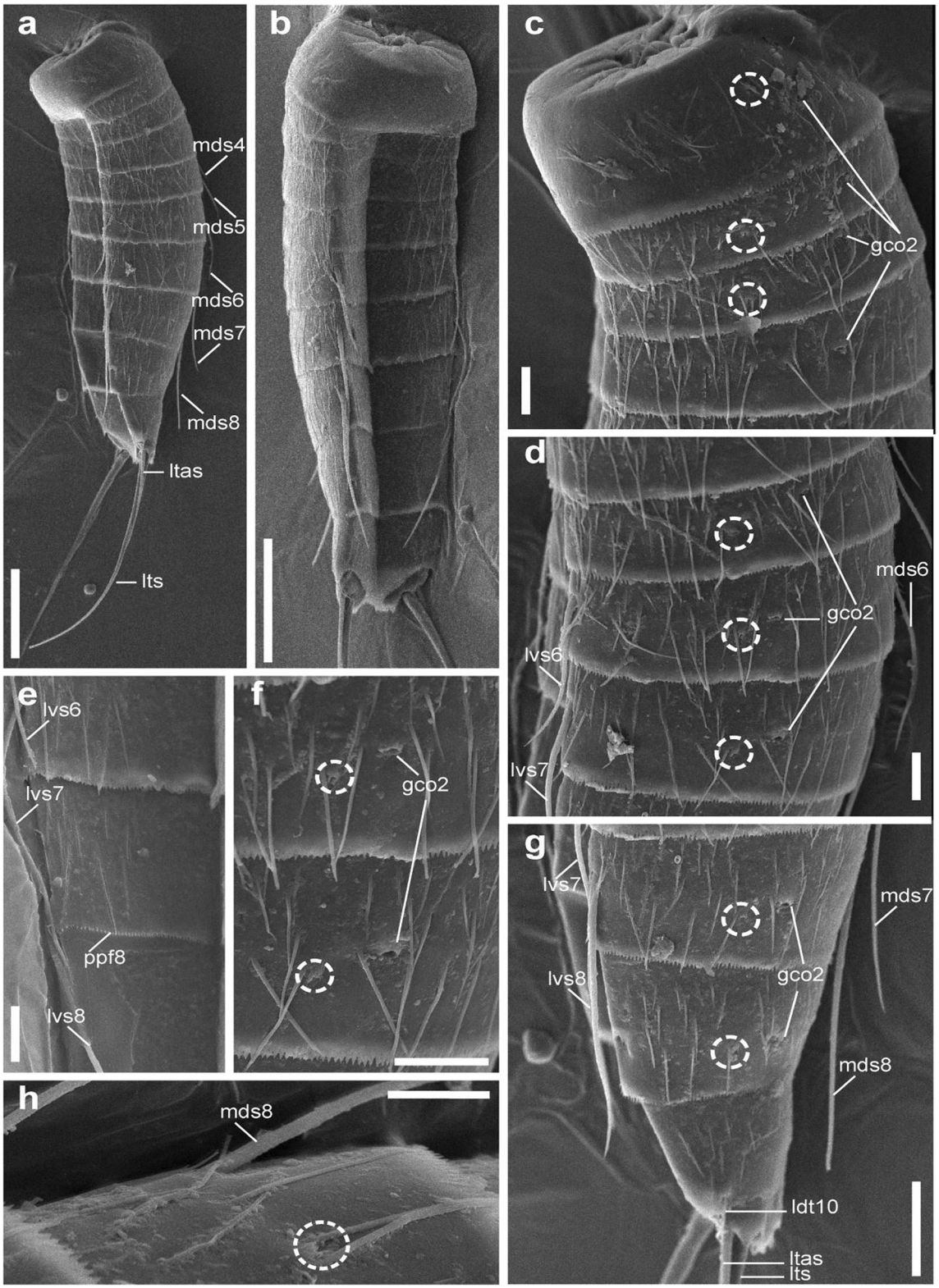

Fig. 8 SEM micrographs of female of *Echinoderes sanctorum* sp. nov., additional material. **a** Lateral overview; **b** ventral overview, **c** left half view of segments 1–4; **d** left half view of segments 5–7; **e** right sternal plate of segments 7–9; **f** detail of type 2 glandular cell outlets and sensory spots of segments 6–7; **g** left half view of segments 8–11; **h** detail of the left paradorsal sensory spot of segment 8. Dashed circles indicate sensory spots. Digits after abbreviations indicate the corresponding segment. Scale bar: **a**, **b** 50 μm; **c**–**f** 10 μm; **g** 20 μm; **h** 5 μm. *gco2* type 2 glandular cell outlet, *ldt* laterodorsal tube, *ltas* lateral terminal accessory spine, *lts* lateral terminal spine, *lvs* lateroventral spine, *mds* middorsal spine, *ppf* primary pectinate fringe

Table 5. Measurements (μm) and proportions of *Echinoderes sanctorum* sp. nov. Numbers in the first column indicate the corresponding segment. *LD* laterodorsal tube, *LTAS* lateral terminal accessory spine, *LTS* lateral terminal spine, *LV* lateroventral spine/tube, *MD* middorsal spine, *MSW* maximum sternal width, measured on segment 7; *n* number of measured specimens, *S* segment length, *SD* standard deviation, *SW* standard width, measured on segment 10; *TL* total trunk length, *VL* ventrolateral tube

	Holotype	*n*	Mean	Range	SD
TL	327	5♀	300	234–377	54.15
MSW 7	74	6♀	70	65–75	4.35
MSW/TL	23%	4♀	24%	20–30%	4.17
SW10	54	4♀	55	51–59	2.96
S1	29	5♀	33	29–41	5.30
S2	29	5♀	26	23–29	2.77
S3	33	5♀	33	30–37	2.49
S4	40	5♀	37	28–51	8.55
S5	35	4♀	40	35–46	4.44
S6	47	4♀	48	41–58	7.06
S7	53	4♀	52	46–61	6.65
S8	57	4♀	59	54–68	6.20
S9	58	4♀	58	52–64	5.09
S10	53	5♀	49	43–55	5.06
S11	30	5♀	29	25–34	3.53
MD4	–	3♀	30	29–31	1.21
MD5	–	4♀	38	34–42	3.29
MD6	–	3♀	40	35–46	5.64
MD7	–	5♀	59	44–70	10.25
MD8	–	3♀	103	97–111	6.86
VL2	–	–	–	–	–
LV5	–	1♀	18	–	–
LV6	45	5♀	41	34–47	6.20
LV7	55	5♀	56	48–64	6.52
LV8	73	7♀	73	68–83	4.93
LV9	75	6♀	76	70–85	5.44
LD10	28	3♀	30	25–37	5.94
LTS	217	5♀	215	185–236	16.52
LTAS	78	5♀	75	62–91	10.60
LTS/TL	67%	5♀	75%	63–93%	11.76
LTAS/TL	24%	5♀	27%	20–39%	8.13
LTAS/LTS	36%	5♀	35%	32–42%	4.05

maximum width at segment 7, progressively tapering toward the last trunk segments; sternal plates relatively narrow compared to the total trunk length, giving the animal a slender appearance. Cuticular hairs acicular, long, non-bracteate, emerging from rounded to oval-shaped perforation sites (Figs. 7j, k and 8a–h). Cuticular hairs distributed in 5–6 straight, transverse rows on segment 1; in 3–4 straight, transverse rows from middorsal to ventrolateral region on segment 2; in 5–7 straight, transverse rows from middorsal to ventrolateral region on segments 3–7 and from paradorsal to ventrolateral region on segments 8 and 9, becoming wavy from the laterodorsal position to the ventral side (Fig. 7j, k); absent on laterodorsal position (except on segment 1) and on the whole segment 11. Primary pectinate fringes straight, strongly serrated, showing a fringe with long tips (Fig. 8c–h). Secondary pectinate fringes absent.

Segment 1 without spines and tubes (Figs. 6a, b; 7a–d; and 8a–c). Unpaired type 1 glandular cell outlet in middorsal position, and paired in lateroventral position (Figs. 6a, b and 7c, d). Paired type 2 glandular cell outlets in subdorsal position (Figs. 6b; 7b, c; and 8c); common size openings, all specimens showing a bilateral pattern on this and the following segments. Two specimens with the outlets in laterodorsal position. Paired sensory spots in subdorsal and midlateral positions, located at the anterior half of the segment (Figs. 6a, b; 7c; and 8c).

Segment 2 with tubes in ventrolateral position (Figs. 6a and 7d). Unpaired type 1 glandular cell outlet in middorsal position and paired ones in ventromedial position (Fig. 6a, b). Paired type 2 glandular cell outlets in laterodorsal position (Figs. 6b; 7b, c; and 8c). Paired sensory spots in paradorsal, laterodorsal and ventromedial positions (Figs. 6a, b; 7c, d; and 8c) Laterodorsal pair of sensory spots not easily observed in most of the specimens.

Segment 3 without spines and tubes (Figs. 6a, b; 7a–d; and 8a-c). Unpaired type 1 glandular cell outlet in middorsal position, and paired in ventromedial position (Figs. 6a, b and 7c). Paired type 2 glandular cell outlets in laterodorsal position (Figs. 6b; 7b, c; and 8c). Paired sensory spots in laterodorsal position (Figs. 6b and 8c).

Segment 4 with a middorsal spine not exceeding half of the plate of the following segment (Figs. 6b; 7c; and 8a). Paired type 1 glandular cell outlets in paradorsal and ventromedial positions (Figs. 6a, b and 7c, d). Paired type 2 glandular cell outlets in laterodorsal position (Figs. 6b; 7b, c; and 8c). Paired sensory spots in subdorsal position (Figs. 6b and 7c).

Segment 5 with a middorsal spine, not exceeding half of the plate of the following segment, and tubes in lateroventral position (Figs. 6a, b; 7c, d, j; and 8a). Unpaired type 1 glandular cell outlets in middorsal position, and paired in ventromedial position (Figs. 6a, b and 7c, d). Paired type 2 glandular cell outlets in laterodorsal position (Figs. 6b; 7b, c, j; and 8d). Paired sensory spots in laterodorsal position (Figs. 6b; 7c, j; and 8d).

Segment 6 with a middorsal spine, not exceeding half of the plate of the following segment, and paired spines in lateroventral position (Figs. 6a, b; 7a, e, f, j; and 8a, b, d). Paired type 1 glandular cell outlets in paradorsal and ventromedial positions (Figs. 6a, b and 7e, f). Paired type 2 glandular cell outlets in laterodorsal position (Figs. 6b; 7b, e, j; and 8d, f). Paired sensory spots in subdorsal and laterodorsal

Table 6 Summary of relevant cuticular characters and positions of *Echinoderes sanctorum* sp. nov. *LA* lateral accessory, *LD* laterodorsal, *LV* lateroventral, *MD* middorsal, *ML* midlateral, *PD* paradorsal, *PV* paraventral, *SD* subdorsal, *VL* ventrolateral, *VM* ventromedial, *ac* acicular spine, *gco1*/2 type 1/2 glandular cell outlet, *ltas* lateral terminal accessory spine, *lts* lateral terminal spine, *pa* papilla, *ps* penile spine, *si* sieve plate, *ss* sensory spot, *t* tube, ♀ female condition of sexually dimorphic characters

Position segment	MD	PD	SD	LD	ML	LA	LV	VL	VM	PV
1	gco1		ss,gco2		ss		gco1			
2	gco1	ss		gco2,ss				t	gco1,ss	
3	gco1			gco2,ss					gco1	
4	ac	gco1	ss	gco2					gco1	
5	ac, gco1			gco2,ss			t		gco1	
6	ac	gco1	ss	gco2,ss			ac		gco1	
7	ac, gco1			gco2,ss			ac	ss	gco1	
8	ac	gco1	ss	gco2,ss			ac		gco1,pa(♀)	
9		gco1,ss		gco2,ss		si	ac	ss	gco1	
10	gco1,gco1		ss	t				ss		gco1
11	gco1, gco1		ss			ltas(♀)	lts			

positions (Figs. 6a, b; 7e, j; and 8d, f). One specimen with ventromedial sensory spots.

Segment 7 with a middorsal spine, reaching half of the tergal plate of the following segment, and paired spines in lateroventral position (Figs. 6a, b; 7a, e, f, j; and 8a, b, d, e, g). Unpaired type 1 glandular cell outlets in middorsal position and paired in ventromedial position (Figs. 6a, b and 7e, f). Paired type 2 glandular cell outlets in laterodorsal position (Figs. 6b; 7b, e, j; and 8d, f). Paired sensory spots in laterodorsal and ventrolateral positions (Figs. 6a, b; 7e, f, j; and 8d, f). Laterodorsal pair of sensory spots apparently absent in one specimen. One specimen with a papilla instead of sensory spot in the right sternal plate and another specimen with likely papillae in ventrolateral position instead of the sensory spots.

Segment 8 with a middorsal spine, reaching half of the tergal plate of the following segment, and paired spines in lateroventral position (Figs. 6a, b; 7a, e–i, k; and 8a, b, e, g, h). Paired type 1 glandular cell outlets in paradorsal and ventromedial positions (Figs. 6a, b and 7e, f). Paired type 2 glandular cell outlets in laterodorsal position (Figs. 6b; 7b, e, g, k; and 8g). Paired sensory spots in laterodorsal position (Figs. 6b; 7e, g, k; and 8g). Sensory spots in subdorsal position could only be undoubtedly observed in the SEM specimen (Fig. 8h). Cuticular structure likely female papillae of undetermined morphology in ventromedial position, close to the type 1 glandular cell outlets (Figs. 6a and 7f, h, k).

Segment 9 with paired lateroventral spines (Figs. 6a and 7a, h, k). Paired type 1 glandular cell outlets in paradorsal and ventromedial positions (Figs. 6a, b and 7h). Paired type 2 glandular cell outlets in laterodorsal position (Figs. 6b; 7b, g, i, k; and 8g). Sensory spots in paradorsal, laterodorsal and ventrolateral positions (Figs. 6a, b; 7g, h, k; and 8g). Nephridiopore as a small sieve plate present in lateral accessory position (Figs. 6a and 7h, k).

Segment 10 with paired, short, narrow laterodorsal tubes (Figs. 6b; 7h, i; and 8g). Two unpaired type 1 glandular cell outlets in middorsal position, and paired in paraventral position (Figs. 6a, b and 7g, h). Paired sensory spots in subdorsal and ventrolateral positions (Figs. 6a, b and 7g, h).

Segment 11 with lateral terminal spines long and slender, distally pointed, showing a hollow central cavity (Figs. 6a, b; 7a, h, i; and 8a, b, g). Females with paired, also conspicuous slender lateral terminal accessory spines, about two to three times shorter than lateral terminal spines (Figs. 6a, b; 7h, i; and 8a-b, g). Tergal and sternal extensions short, distally rounded (Figs. 6a, b; 7a, h; and 8b, g). Two unpaired type 1 glandular cell outlets in middorsal position (Fig. 6b). Paired sensory spots in subdorsal position (Figs. 6b and 7g).

Echinoderes zeppilliae sp. nov.

http://zoobank.org/C0FEF431-7834-43F6-9CCA-D14AF6D9FFAD (Figs. 9 and 10 and Tables 2, 7, and 8)

Synonymy *Echinoderes* sp. 3 (in Sánchez et al. 2019).

Material examined Holotype, adult female, collected on 3 May 2016 at the Clarion-Clipperton Fracture Zone (central-eastern Pacific Ocean), BGR license area: 11°51.284′ N, 117°02.365′ W (Table 2) at 4135 m depth; mounted in Fluoromount G®, deposited at MfN under accession number: 12447. Paratypes, four adult females collected at different stations than the holotype (see Table 2), mounted in Fluoromount G® and stored at MfN under accession numbers: ZMB 12448-12451.

Etymology The species is named after Dr Daniela Zeppilli, colleague, friend and expert researcher on meiofauna from

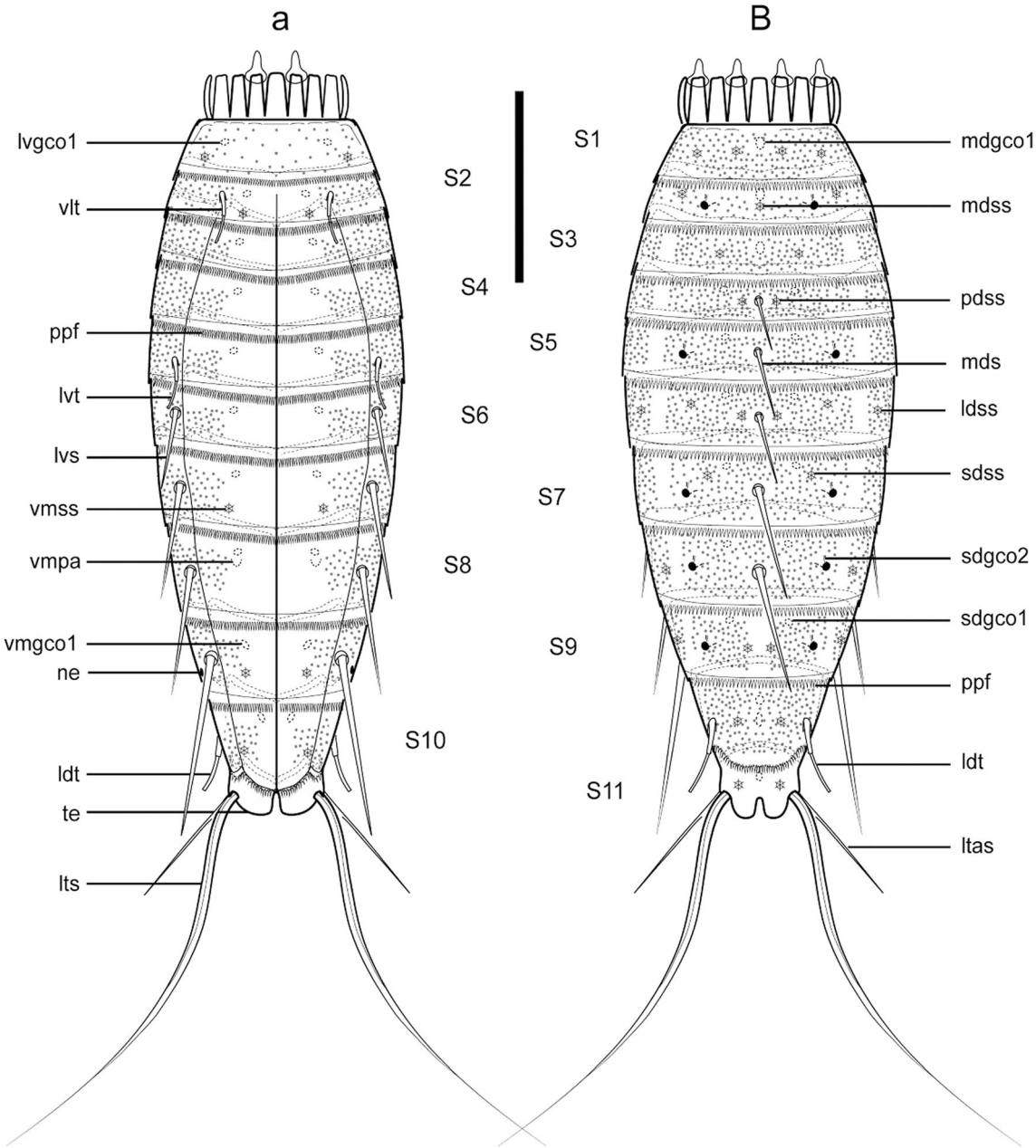

Fig. 9 Line art illustrations of *Echinoderes zeppilliae* sp. nov. **a** Female, ventral view; **b** female, dorsal view. Scale bar: 100 µm. *ldss* laterodorsal sensory spot, *ldt* laterodorsal tube, *ltas* lateral terminal accessory spine, *lts* lateral terminal spine, *l-vgco1* lateroventral type 1 glandular cell outlet, *lvs* lateroventral spine, *lvt* lateroventral tube, *mdgco1* middorsal type 1 glandular cell outlet, *mds* middorsal spine, *mdss* middorsal sensory spot, *ne* nephridiopore, *pdss* paradorsal sensory spot, *ppf* primary pectinate fringe, *S1–S11* trunk segment, *sdgco1* subdorsal type 1 glandular cell outlet, *sdgco2* subdorsal type 2 glandular cell outlet, *sdss* subdorsal sensory spot, *te* tergal extension, *vlt* ventrolateral tube, *vmgco1* ventromedial type 1 glandular cell outlet, *vmpa* ventromedial papilla, *vmss* ventromedial sensory spot

extreme environments, currently working on nematodes from the CCZ French area.

Diagnosis *Echinoderes* with spines in middorsal position on segments 4–8 and lateroventral position on segments 6–9, increasing in length posteriorly; tubes in ventrolateral position on segment 2, in lateroventral position on segment 5 and in laterodorsal position on segment 10; bilateral type 2 glandular cell outlets in subdorsal position on segments 2, 5 and 7–9; tergal extensions short, distally rounded.

Description See Table 7 for measurements and dimensions, and Table 8 for summary of spine, tube, nephridiopore, glandular cell outlet, female papilla, and sensory spot locations.

Head with retractable mouth cone and introvert. None of the examined specimens had the introvert everted, hence

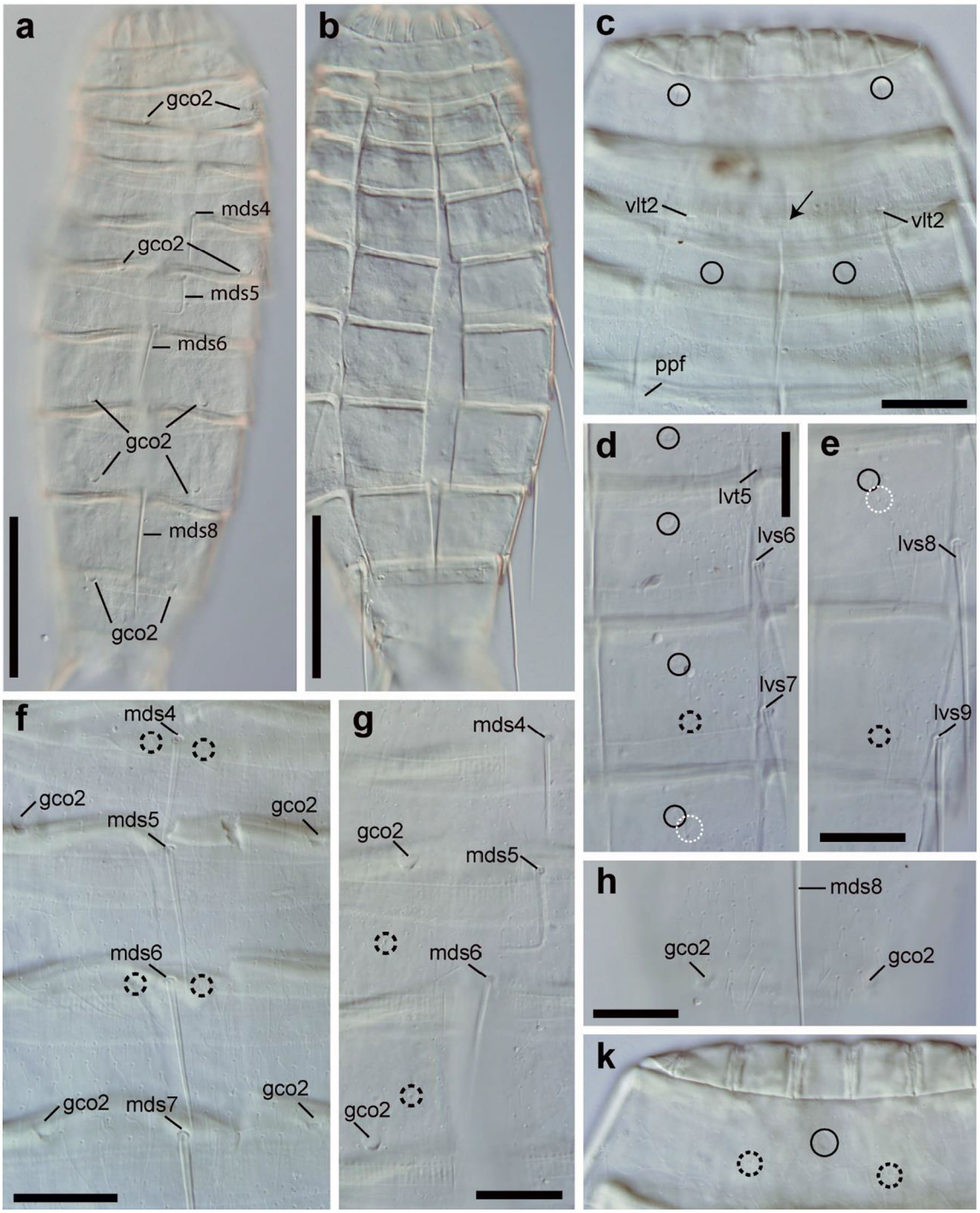

Fig. 10 DIC photographs of *Echinoderes zeppilliae* sp. nov. **a**, **d**–**e**, **g**–**i** Paratypic female. **b**, **j** Holotypic female. **c**, **f**, **k** Paratypic female. **a** Dorsal overview; **b** ventral overview; **c** ventral view of neck and segments 1–4; **d** left sternal plates of segments 5–8; **e** left sternal plates of segments 8–9; **f** dorsal view of segments 4–7, from middorsal to subdorsal positions; **g** dorsal view of left half of segments 4–7, from middorsal to subdorsal positions; **h** dorsal view of segment 9; **i** segments 10–11; **j** dorsal view of segments 7–8, from middorsal to subdorsal positions; **k** dorsal view of segments 1–3. Dashed black circles indicate sensory spots. Dashed white circles indicate female papillae. Closed circles indicate type 1 glandular cell outlets. Dashed line indicates midventral division of segment 2. Digits after abbreviations indicate the corresponding segment. Scale bar: **a**–**b**, 100 μm; **c**–**j**, 25 μm. *gco2* type 2 glandular cell outlet, *ldt* laterodorsal tube, *ltas* lateral terminal accessory spine, *lvs* lateroventral spine, *lvt* lateroventral tube, *mds* middorsal spine, *ppf* primary pectinate fringe, *vlt* ventrolateral tube

details on oral style and scalid morphology and arrangement cannot be provided.

Neck with sixteen elongated, trapezoidal placids, wider at base, approximately two to three times longer than wide, with

Table 7 Measurements (μm) and proportions of *Echinoderes zeppilliae* sp. nov. Numbers in the first column indicate the corresponding segment. *LD* laterodorsal tube, *LTAS* lateral terminal accessory spine, *LTS* lateral terminal spine, *LV* lateroventral spine/tube, *MD* middorsal spine, *MSW* maximum sternal width, measured on segment 7; *n* number of measured specimens, *S* segment length, *SD* standard deviation, *SW* standard width, measured on segment 10; *TL* total trunk length, *VL* ventrolateral tube

	Holotype	n	Mean	Range	SD
TL	372	5♀	386	357–426	27.61
MSW 7	106	4♀	98	93–106	5.62
MSW/TL	29%	4♀	25.35%	23–29%	2.56
SW10	75	4♀	73	71–75	2.07
S1	35	4♀	42	35–50	6.94
S2	29	4♀	36	29–41	5.39
S3	40	4♀	39	34–42	3.63
S4	39	4♀	44	39–50	5.70
S5	48	4♀	50	43–56	6.05
S6	60	4♀	60	57–61	1.76
S7	67	3♀	67	66–67	0.49
S8	65	3♀	69	65–74	4.13
S9	72	3♀	71	70–72	1.36
S10	54	3♀	54	54–54	0.36
S11	39	3♀	39	37–40	1.80
MD4	31	3♀	31	29–33	1.75
MD5	36	4♀	37	35–40	2.19
MD6	42	5♀	40	35–42	2.87
MD7	66	3♀	65	63–66	1.31
MD8	–	3♀	86	83–88	2.53
VL2	10	4♀	20	10–31	9.38
LV5	36	5♀	25	13–36	9.08
LV6	47	5♀	46	44–49	1.95
LV7	63	5♀	64	62–69	3.08
LV8	79	5♀	80	73–86	4.81
LV9	95	5♀	94	89–102	5.19
LD10	29	3♀	42	29–61	16.57
LTS	242	4♀	228	216–242	12.06
LTAS	69	5♀	71	68–76	3.31
LTS/TL	65%	4♀	58%	51–65%	5.89
LTAS/TL	19%	5♀	19%	16–21%	1.72
LTAS/LTS	29%	4♀	31%	29–32%	1.67

a distinct joint between the neck and segment 1 (Figs. 9a, b and 10a–c, k); midventral one widest (ca. 16–18 μm wide at base), remaining ones narrower (10–12 μm wide at base) (Figs. 9a, b and 10a–c, k). Placids closely situated at base with distal cuticular folds between adjacent ones. A ring of six short, hairy trichoscalids associated with the placids of the neck is present, attached to small, three-lobed trichoscalid plates (Fig. 9a, b).

Trunk with eleven segments (Figs. 9a, b and 10a, b). Segments 1–2 as closed cuticular rings, segment 2 as circular ring with a partial midventral division, remaining ones with one tergal and two sternal cuticular plates (Figs. 9a, b and 10a–c). Tergal plates of anterior segments slightly bulging middorsally, posterior ones more flattened, giving the animal a tapering outline in lateral view. Sternal plates reach their maximum width at segment 7, progressively tapering toward the last trunk segments; sternal plates relatively narrow compared to the total trunk length. Cuticular hairs acicular, long, emerging from rounded to oval-shaped perforation sites. Dorsal cuticular hairs distributed in 3–4 and 5–6 straight, transverse rows on segments 1–4 and 5–10 respectively; with longitudinal, laterodorsal bald bands on segments 3–10 (Figs. 9b and 10f–g); segment 9 furthermore with a longitudinal, middorsal bald band (Figs. 9b and 10h). Ventral cuticular hairs distributed in 4–5 more wavy transverse rows extending up to the ventromedial glandular cell outlets type 1; absent in paraventral position and on segment 11 (Figs. 9a and 10c, d, e). Primary pectinate fringes straight, strongly serrated, showing a fringe with long tips (Fig. 9a, b). Secondary pectinate fringes not detected.

Segment 1 without spines and tubes (Figs. 9a, b and 10a–c, k). Unpaired type 1 glandular cell outlet in middorsal position, and paired type 1 glandular cell outlets in lateroventral position (Figs. 9a, b and 10c, k). Paired sensory spots in paradorsal, laterodorsal and sublateral positions, located at the anterior half of the segment, except the latter that are situated at the middle region of the plate (Figs. 9a, b and 10k).

Segment 2 with a partial midventral division and tubes in ventrolateral position (Figs. 9a and 10c). Unpaired type 1 glandular cell outlet in middorsal position, and paired ones in ventromedial position (Fig. 9a, b). Paired type 2 glandular cell outlets in subdorsal position, common size openings (Figs. 9b and 10a, k); all specimens show a bilateral pattern of type 2 glandular cell outlets on this and the following segments. Unpaired sensory spot in middorsal position, and paired ones in laterodorsal and ventromedial positions (Figs. 9a, b and 10k).

Segment 3 without spines and tubes (Figs. 9a, b and 10a–c, k). Unpaired type 1 glandular cell outlet in middorsal position, and paired ones in ventromedial position (Figs. 9a, b and 10c). Paired sensory spots in subdorsal position (Figs. 9b and 10k).

Segment 4 with a middorsal spine not exceeding half of the plate of the following segment (Figs. 9b and 10a, f–g). Paired type 1 glandular cell outlets in subdorsal and ventromedial positions (Fig. 9a, b). Paired sensory spots in paradorsal position (Figs. 9b and 10f).

Segment 5 with a middorsal spine, not exceeding half of the plate of the following segment, and tubes in lateroventral position (Figs. 9a, b and 10a, d, f, g). Paired type 1 glandular cell outlets in subdorsal and ventromedial positions (Figs. 9a, b and 10d). Paired type 2 glandular cell outlets in laterodorsal position (Figs. 9b and 10f, g).

Table 8 Summary of relevant cuticular characters and positions of *Echinoderes zeppilliae* sp. nov. *LA* lateral accessory, *LD* laterodorsal, *LV* lateroventral, *MD* middorsal, *PD* paradorsal, *PV* paraventral, *SD* subdorsal, *SL* sublateral, *VL* ventrolateral, *VM* ventromedial, *ac* acicular spine, *gco1*/2 type 1/2 glandular cell outlet, *ltas* lateral terminal accessory spine, *lts* lateral terminal spine; pa, papilla, *ps* penile spine, *si* sieve plate, *ss* sensory spot, *t* tube, ♀ female condition of sexually dimorphic characters

Position segment	MD	PD	SD	LD	SL	LA	LV	VL	VM	PV
1	gco1	ss		ss	ss		gco1			
2	gco1,ss		gco2	ss				t	gco1,ss	
3	gco1		ss						gco1	
4	ac	ss	gco1						gco1	
5	ac		gco1, gco2				t		gco1	
6	ac	ss	gco1,ss	ss			ac		gco1	
7	ac		gco1, gco2,ss				ac		gco1,ss	
8	ac		gco1, gco2	ss			ac		gco1,pa(♀)	
9		ss	gco1, gco2	ss	si		ac		gco1,ss	
10	gco1,gco1		ss	t				ss		gco1
11	gco1		ss			ltas(♀)	lts			

Segment 6 with a middorsal spine, not exceeding half of the plate of the following segment, and paired spines in lateroventral position (Figs. 9a, b and 10a, d, f, g). Paired type 1 glandular cell outlets in subdorsal and ventromedial positions (Figs. 9a, b and 10d). Paired sensory spots in paradorsal, subdorsal and laterodorsal positions (Figs. 9b and 10f, g).

Segment 7 with a middorsal spine, almost reaching the edge of the tergal plate of the following segment, and paired spines in lateroventral position (Figs. 9a, b and 10a, d, f, j). Paired type 1 glandular cell outlets in subdorsal and ventromedial positions (Figs. 9a, b and 10d). Paired type 2 glandular cell outlets in laterodorsal position, aligned with those of segment 5 (Figs. 9b and 10f, g). Paired sensory spots in subdorsal and ventromedial positions, the former located aligned with those of the previous segment and anterior to the type 2 glandular cell outlets (Figs. 9a, b and 10d, g).

Segment 8 with a middorsal spine, reaching the edge of the tergal plate of the following segment, and paired spines in lateroventral position (Figs. 9a, b and 10a, e, h, j). Paired type 1 glandular cell outlets in subdorsal and ventromedial positions (Figs. 9a, b and 10e). Paired type 2 glandular cell outlets in laterodorsal position, aligned with those of the previous segment (Figs. 9b and 10j). Paired sensory spots in laterodorsal position, slightly posterior to the type 2 glandular cell outlets (Fig. 9b). Paradorsal sensory spots could not be observed. Female, sexually dimorphic papillae in ventromedial position, located near to the type 1 glandular cell outlets (Figs. 9a and 10d, e); detailed morphology of these papillae not determined.

Segment 9 with paired lateroventral spines (Figs. 9a and 10e). Paired type 1 glandular cell outlets in subdorsal and ventromedial positions, the latter ones more oval than previous ones (Fig. 9a, b). Paired type 2 glandular cell outlets in laterodorsal position (Figs. 9b and 10h). Sensory spots in paradorsal, laterodorsal, and ventromedial positions (Figs. 9a, b and 10e). Nephridiopore as a small sieve plate present in sublateral position (Fig. 9a).

Segment 10 with paired, long, narrow laterodorsal tubes (Figs. 9b and 10i). Two unpaired type 1 glandular cell outlets in middorsal position, and with oval, paired type 1 glandular cell outlets in paraventral position (Fig. 9a, b). Paired sensory spots in subdorsal and ventrolateral positions (Fig. 9b).

Segment 11 with lateral terminal spines long and slender, distally pointed, showing a hollow central cavity (Fig. 9a, b). Females with paired, also slender lateral terminal accessory spines, about three times shorter than lateral terminal spines (Figs. 9a, b and 10i). Tergal and sternal extensions short, distally rounded (Fig. 9a, b). Unpaired type 1 glandular cell outlet in middorsal position (Fig. 9b). Paired sensory spots in subdorsal position (Fig. 9b).

Morphological diversity of Kinorhyncha

Clarion-Clipperton Fracture Zone

In the BGR contract area, densities of 0.4 ± 0.2 total kinorhynch specimens per 10 cm^{-2} (mean per core of 2.7 ± 1.7 specimens), 0.1 ± 0.1 adults per 10 cm^{-2} (mean per core of 0.6 ± 0.7 specimens), and 0.3 ± 0.2 juveniles per 10 cm^{-2} (mean per core of 2.2 ± 1.6 specimens) were registered. Of the 558 kinorhynch specimens collected from the BGR area, ca. 80% were juveniles (Fig. 11) and therefore unidentified to the species level. Concerning the 116 adult specimens, 112 could be morphologically identified to species level, yielding 12 species belonging to seven families and 10 genera (including the new species described herein) (H′ 1.9; J′ 0.3) (Figs. 12 and 13 and Online supplements):

- *Echinoderes* Claparède, 1863: two new, still undescribed species; *E. delaordeni* sp. nov., *E. sanctorum* sp. nov., *E. zeppilliae* sp. nov., and the recently described *E. shenlong* from the CCZ (Sánchez et al. 2019).

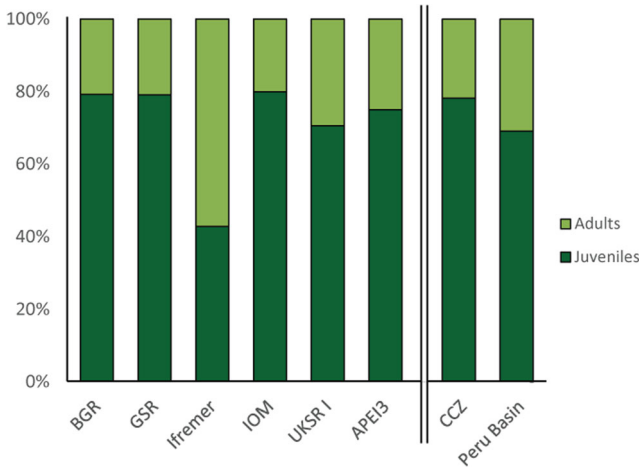

Fig. 11 Barplot showing the relative abundance of juveniles in relation to the total kinorhynch community in the CCZ, including all contract areas; and in the whole CCZ and the Peru Basin

- *Cephalorhyncha* Adrianov, 1999 in Adrianov & Malakhov 1999: one recently described species from the CCZ, *C. polunga* (Sánchez et al. 2019).
- *Meristoderes* Herranz et al., 2012 one recently described species from the CCZ, *M. taro* (Sánchez et al. 2019).
- *Semnoderes* Zelinka, 1907: one new, still undescribed species; and *S. pacificus* Higgins, 1967 (Higgins 1967; Sánchez et al. 2019).
- *Campyloderes* Zelinka, 1907: *Campyloderes* cf. *vanhoeffeni*.
- *Fissuroderes* Neuhaus & Blasche, 2006: *Fissuroderes higginsi* Neuhaus & Blasche, 2006 (Neuhaus and Blasche 2006; Sánchez et al. 2019).

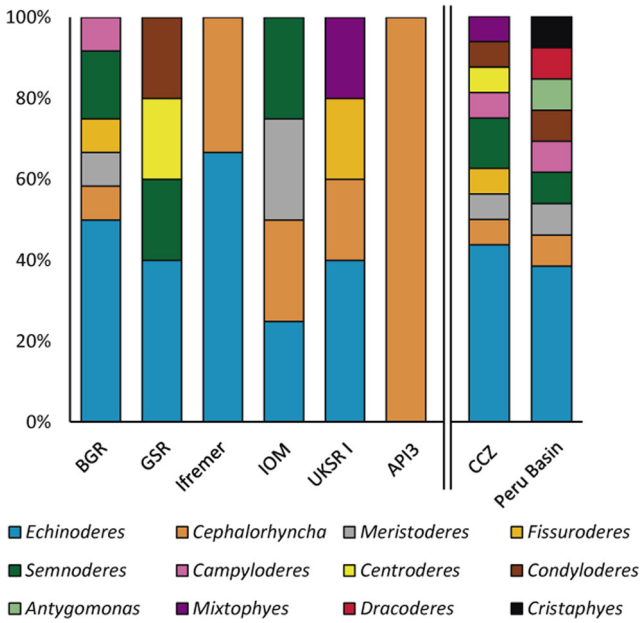

Fig. 12 Barplot showing the relative abundance of kinorhynch' genera reported in the CCZ, including all contract areas; and in the whole CCZ and the Peru Basin

Therefore, the current kinorhynch knowledge for the BGR contract area encompasses nine undescribed or recently described species, plus three already known species. Regarding the kinorhynch assemblage, *Echinoderes* is the most diverse genus in the BGR area (six species), followed by *Semnoderes* (two species), whereas the remaining four genera, namely *Cephalorhyncha*, *Campyloderes*, *Fissuroderes*, and *Meristoderes*, are represented by single species (Fig. 12). *Echinoderes* sp. 4 is the most abundant species so far (45 specimens in 33 stations), followed by *Cephalorhyncha polunga* (15 specimens in 12 stations), *Echinoderes delaordeni* sp. nov. (12 specimens in 10 stations), and *M. taro* (11 specimens in six stations) (Fig. 13 and see Online supplements for specific locations). Contrarily, two species are known from the area only as single reports, namely *Echinoderes* sp. 6 and *Semnoderes* sp.1 (see Online supplements for specific locations).

One hundred eleven kinorhynch specimens were collected from the remaining contract areas studied herein and from APEI3, of which 30 were adults and could be subsequently identified to the species level (Figs. 12-13 and Online supplements):

- GSR contract area: Densities of 0.7 ± 0.3 of total kinorhynch specimens per 10 cm^2 (mean per core of 4.8 ± 2.3 specimens), 0.2 ± 0.1 adults per 10 cm^{-2} (mean per core of 1.0 ± 0.7 specimens) and 0.6 ± 0.2 juveniles per 10 cm^{-2} (mean per core of 3.8 ± 1.6 specimens) were registered. Five adult specimens belonging to five species were identified (ca. 80% were juveniles; see Fig. 11) (H′ 1.6; J′ 0.5): *Condyloderes kurilensis* Adrianov & Maiorova, 2016 (Adrianov and Maiorova 2016; Sánchez et al. 2019), *Echinoderes juliae* Sørensen et al., 2018 (Sørensen et al. 2018) present as a single report in this area within the CCZ (Sánchez et al. 2019), *Echinoderes delaordeni* sp. nov., *Semnoderes pacificus* (Sánchez et al. 2019), and one *Centroderes* specimen that could not be identified to the species level.
- Ifremer contract area: Densities of 0.2 ± 0.1 of total kinorhynch specimens per 10 cm^{-2} (mean per core of 1.4 ± 0.5 specimens), 0.1 ± 0.1 adults per 10 cm^{-2} (mean per core of 0.8 ± 0.8 specimens) and 0.1 ± 0.1 juveniles per 10 cm^{-2} (mean per core of 0.6 ± 0.9 specimens) were registered. Four adult specimens belonging to three species were identified (ca. 43% were juveniles; see Fig. 11) (H′ 1.0; J′ 0.6): *Cephalorhyncha polunga*, *Echinoderes sanctorum* sp. nov., and a new, still undescribed species, *Echinoderes* sp. 4.
- IOM contract area: Densities of 0.45 ± 0.1 of total kinorhynch specimens per 10 cm^{-2} (mean per core of 3.1 ± 1.0 specimens), 0.1 ± 0.1 adults per 10 cm^{-2} (mean per core of 0.6 ± 0.7 specimens), and 0.4 ± 0.2 juveniles per 10 cm^{-2} (mean per core of 2.5 ± 1.3 specimens) were

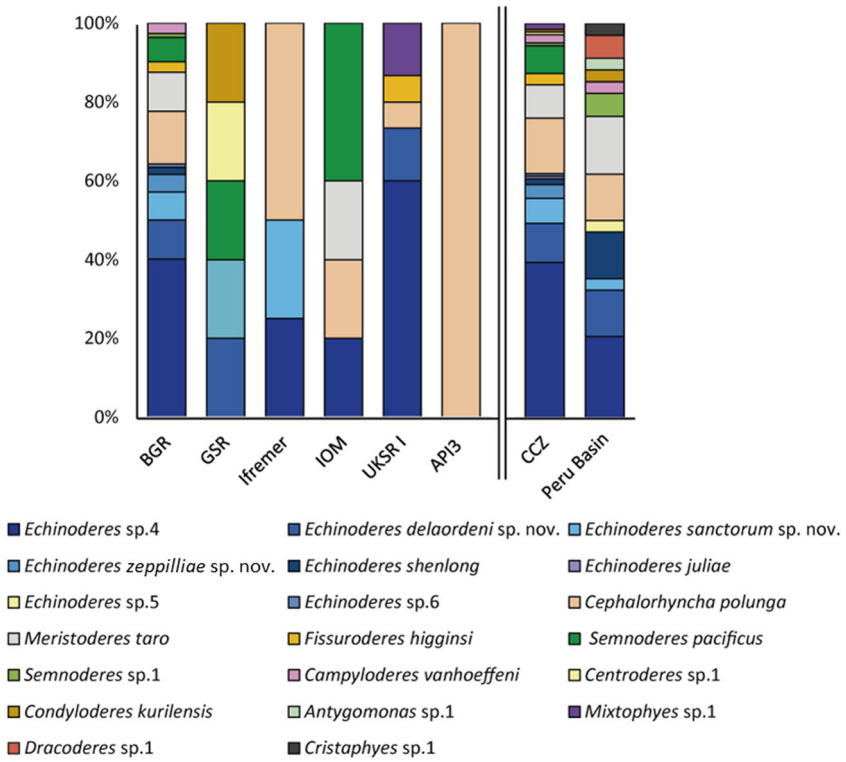

Fig. 13 Barplot showing the relative abundance of species in the CCZ, including all contract areas; and in the whole CCZ and the Peru Basin

registered. Five adult specimens belonging to four species were identified (ca. 80% were juveniles; see Fig. 11) (H′ 1.3; J′ 0.5): *Semnoderes pacificus*, *Meristoderes taro*, *Cephalorhyncha polunga*, and *Echinoderes* sp. 4, a new, still undescribed species (Sánchez et al. 2019).

- UKSR I contract area: Densities of 0.3 ± 0.1 of total kinorhynch specimens per 10 cm^{-2} (mean per core of 1.8 ± 0.9 specimens), 0.1 ± 0.1 adults per 10 cm^{-2} (mean per core of 0.5 ± 0.7 specimens), and 0.2 ± 0.2 juveniles per 10 cm^{-2} (mean per core of 1.3 ± 1.1 specimens) were registered. 15 adult specimens belonging to five species were identified (ca. 71% were juveniles; see Fig. 11) (H′ 1.2; J′ 0.4): *Cephalorhyncha polunga*; *Fissuroderes higginsi*, *Echinoderes delaordeni* sp. nov. and two still undescribed species, *Echinoderes* sp. 4, and *Mixtophyes* sp.1 (Sánchez et al. 2019).
- APEI3 (Area of Particular Environmental Interest number 3): Densities of 0.2 ± 0.1 of total kinorhynch specimens per 10 cm^{-2} (mean per core of 1.3 ± 0.6 specimens), 0.1 ± 0.1 adults per 10 cm^{-2} (mean per core of 0.3 ± 0.6 specimens), and 0.1 ± 0.1 juveniles per 10 cm^{-2} (mean per core of 1.0 ± 1.0 specimens) were registered. Only one adult specimen of *Cephalorhyncha polunga* was found (ca. 75% were juveniles; see Fig. 11) (H′ 0.0).

Once again, *Echinoderes* sp. 4 is the most abundant species considering these six contract areas (11 specimens at nine stations), followed by *Cephalorhyncha polunga* (five specimens at five stations), *Echinoderes delaordeni* sp. nov. (three specimens at three stations), and *Semnoderes pacificus* (three specimens at three stations) (Fig. 13 and Online supplements for specific locations). Except for *Mixtophyes* sp.1, the remaining species are known from the referred areas only as single reports, namely *Echinoderes* sp. 6, *Fissuroderes higginsi*, *Echinoderes juliae*, *Echinoderes sanctorum* sp. nov, *Meristoderes taro*, *Centroderes* sp.1, *Condyloderes kurilensis* (see Online supplements for specific locations).

Analyses showed statistically significant differences in densities of total kinorhynch specimens (KW test, p = 1.909e-06), adults (KW test, p = 0.002), and juveniles (KW test, p = 3.104e-05) between areas. The pairwise comparison test showed that APEI3, the UKSR I and the Ifremer areas shared similar densities of total kinorhynchs, adults and juveniles, which were significantly lower than in the other CCZ areas. Specifically, the GSR area had significantly higher densities of total kinorhynchs and juveniles than in the other studied areas (KW test, $p < 0.04$); the BGR area only had significantly higher densities of total kinorhynchs and juveniles compared to the Ifremer and the UKSR I areas; the IOM area had significantly higher densities of total kinorhynchs and juveniles than the Ifremer, the UKSR I and APEI3 areas (KW test, $p < 0.02$), except density of juveniles in APEI3. These analyses also showed that all contract areas in the CCZ had similar adult densities (KW test, $p > 0.05$), but if

the total density of kinorhynchs differed significantly, it always occurred together with differences in the density of juveniles as well (see Fig. 14 and Online supplements).

Considering all the studied contract areas together, the kinorhynch community in the CCZ reached densities of 0.4 ± 0.2 of total kinorhynch specimens per 10 cm^{-2} (mean per core of 2.6 ± 1.7 specimens), 0.1 ± 0.1 adults per 10 cm^{-2} (mean per core of 0.6 ± 0.7 specimens), and 0.3 ± 0.2 juveniles per 10 cm^{-2} (mean per core of 2.1 ± 1.6 specimens), being composed of a total of 16 morphospecies (Fig. 13) (H′ 2.0; J′ 0.3), with most of the aforementioned species also being present in the BGR contract area, except for *Mixtophyes* sp.1 (UKSR I), *Centroderes* sp.1, *Condyloderes kurilensis*, and *Echinoderes juliae* (GSR). No correlations were found between males, females, and juveniles neither between the different kinorhynch species present in the CCZ.

Peru Basin

Of the 110 kinorhynch specimens collected from the reference area of the DEA, ca. 69% were juveniles (Fig. 11), and could not be identified to the species level. The 34 adult specimens, contrarily, could be identified to the lowest taxonomic level (H′ 2.3; J′ 0.3). Seven of them were also present in the CCZ (Figs. 12-13 and Online supplements): *Cephalorhyncha polunga*, *Meristoderes taro*, *Echinoderes delaordeni* sp. nov., *Echinoderes sanctorum* sp. nov., *Echinoderes* sp.4, *Semnoderes* sp.1, and *Campyloderes* cf. *vanhoeffeni*. *Echinoderes shenlong* was previously reported from the Peru Basin (Sánchez et al. 2019), but new observations suggest that these records may belong to a different but morphologically very similar species (pers. obs. Dr. Hiroshi Yamasaki). The remaining five species from the Peru Basin have not yet been observed in the CCZ (Fig. 13): four exclusive, undescribed species so far, namely *Antygomonas* sp.1, *Dracoderes* sp.1 (identified as *D.* cf. *toyoshioae* Yamasaki, 2015 in Sánchez et al. 2019), *Echinoderes* sp.5 and *Cristaphyes* sp.1; together with *Condyloderes kurilensis*.

The kinorhynch community from the reference area of the DEA reached densities of 0.6 ± 0.3 of total kinorhynch specimens per 10 cm^{-2} (mean per core of 4.2 ±2.1 specimens), 0.1 ± 0.1 adults per 10 cm^{-2} (mean per core of 0.6 ±1.1 specimens) and 0.3 ± 0.2 juveniles per 10 cm^{-2} (mean per core of 2.9 ±1.6 specimens). No correlations were found between males, females and juveniles neither between the different kinorhynch species in the Peru Basin. Statistical analyses showed significant differences between the kinorhynch community inhabiting the CCZ and the Peru Basin in terms of total specimen, adult, and juvenile density (p = 5.828 e-05; p = 4.279 e-05; p = 0.006) (see Fig. 14).

DNA-based diversity of Kinorhyncha

Out of the 253 samples analyzed from the CCZ area, Kinorhyncha ASVs were only detected in 15 samples from three cruises and six areas: one station in the IRA1 area, eight

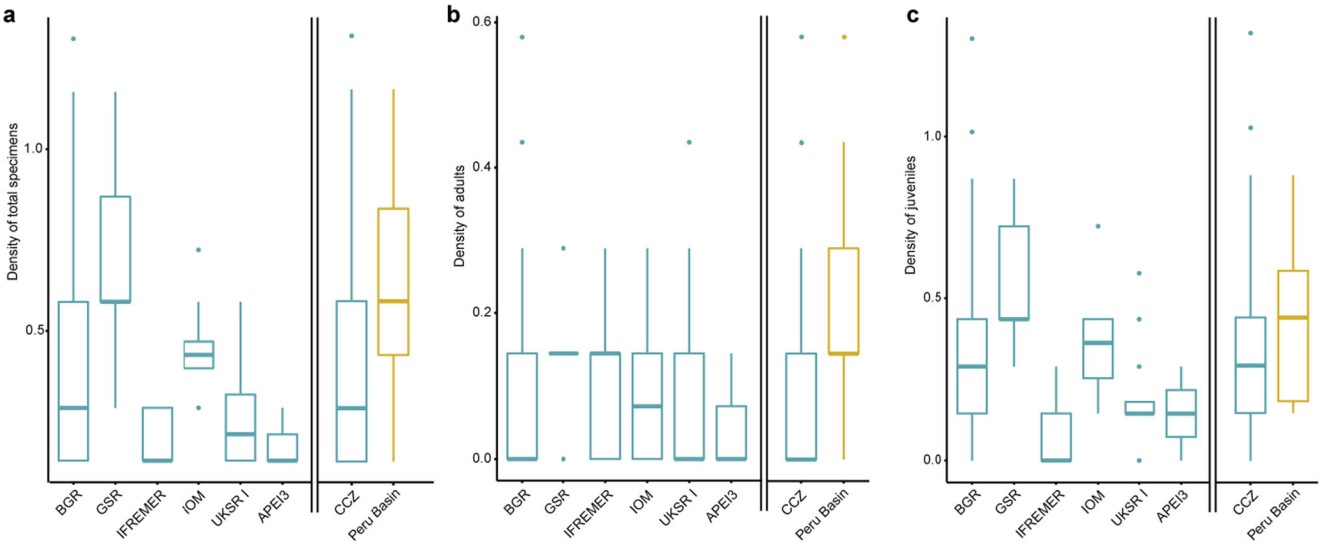

Fig. 14 Kinorhynch community structure at each contract area and APEI3 of the CCZ (blue), and in the whole CCZ (including all the contract areas, blue) and the Peru Basin (yellow). **a** Density of total specimens (including adults and juveniles); **b** density of adult specimens; **c** density of juvenile specimens. Boxplots represent the median value (horizontal line within the box), the distributions of 50% of the data (the box), and the highest and lowest values within 95% of the distribution (the whisker)

stations in IOM (three), GSR (three) and IRA Trial (two) areas, and six stations in the BGR Trial (two) and BGR Reference (four) areas; while no kinorhynch ASVs were detected in the other areas of the CCZ (see Table 9). Amplicon sequencing of the V1&V2 hypervariable region of the 18S rRNA gene yielded 624 reads that matched to Kinorhyncha based on GenBank taxonomic assignments and eventually resulted in 14 ASVs. Of these, six blasted with different kinorhynch species from the NCBI database. These species found in the CCZ area include *Cephalorhyncha* sp., *Condyloderes* sp., *Echinoderes ajax* Sørensen, 2014, *E. rex* Lundbye et al., 2011, *Semnoderes armiger* Zelinka, 1928, and *Zelinkaderes brightae* Sørensen et al., 2007 (Lundbye et al. 2011; Sørensen 2014; Sørensen et al. 2007; Zelinka 1928) (Table 10). All detected kinorhynch ASVs had a grade value higher than 98% (Fig. 15), which further ensures taxonomic assignments with high precision.

Out of the species detected, the most widespread ASV was *Semnoderes armiger*, recovered at six stations (out of 15) from three CCZ areas (see Fig. 16): BGR Trial, BGR Reference, and IOM; whereas *Zelinkaderes brightae* was collected at one station in the IOM, BGR Reference, and IRA1areas, despite the low number of reads in the two latter areas. On the other hand, the genus *Cephalorhyncha* showed the highest diversity, with 5 ASVs detected in the CCZ, followed by the members of *Echinoderes*, which was represented by 4 ASVs. The phylogenetic tree from the kinorhynch ASVs of the CCZ area showed a distinct clustering pattern, with high posterior probabilities of different kinorhynch species according to GenBank taxonomic assignments (Fig. 17). Regarding the composition of kinorhynch ASVs among the six defined areas (Fig. 18, Table 10), the highest richness was observed in the GSR area (with seven different ASVs), followed by the IOM area (with six different ASVs). The BGR Reference area brought three different ASVs of which one is unique to this area (*Semnoderes armiger* ASV number 22242). Two different ASVs were detected in the IRA Trial area, including one unique ASV (*Echinoderes ajax* ASV number 12177). There is one common kinorhynch ASV revealed from the BGR Trial and BGR Reference areas as well as the IOM (*Semnoderes armiger* ASV number 8122). Only one ASV was detected from the IRA1 area which is shared with the IRA Trial area (*Zelinkaderes brightae* ASV number 17043).

Discussion

Notes on diagnostic features in *Echinoderes zeppilliae* sp. nov., *Echinoderes delaordeni* sp. nov., and *Echinoderes sanctorum* sp. nov.

The three new species are easily distinguished from their congeners by the combination of two conspicuous features: middorsal spines from segments 4 to 8 and type 2 glandular cell outlets on most trunk segments. Specifically, *Echinoderes sanctorum* sp. nov. has the largest number of type 2 glandular cell outlets, from segments 1 to 9. *Echinoderes ohtsukai* Herranz & Leander, 2016 is the only congener characterized by the presence of this kind of outlets in most of the segments so far. Thus, *E. ohtsukai* has type 2 glandular cell outlets on segments 2–9, being absent on segment 1 (Herranz and Leander 2016). Moreover, *E. ohtsukai* has a middorsal spine only on segment 4 (vs. middorsal spines of *Echinoderes*

Table 9 List of the CCZ stations in which kinorhynch ASVs were detected

DNA extraction ID	Cruise	Databank ID	Area	Core	Station	Fixative	Latitude	Longitude
121	KM14-08, Mangan 2014	85	IRA1 8	8	8	DESS	11° 47.400′ N	117° 32.740′ W
72	SO239, JPIO/CCZ 2015	124	GSR 4	11	896	DESS	13° 51.28′ N	123° 14.69′ W
73	SO239, JPIO/CCZ 2015	125	GSR 7	8	912	DESS	13° 51.06′ N	123° 14.22′ W
74	SO239, JPIO/CCZ 2015	141	GSR 6	8	1041	DESS	13° 50.80′ N	123° 04.66′ W
69	SO239, JPIO/CCZ 2015	104	IOM 4	12	793	DESS	11° 03.89′ N	119° 39.18′ W
67	SO239, JPIO/CCZ 2015	92	IOM 11	4	602	DESS	11° 04.38′ N	119° 39.35′ W
58	SO239, JPIO/CCZ 2015	86	IOM 14	1	527	DESS	11° 45.02′ N	119° 39.81′ W
65	SO239, JPIO/CCZ 2015	64	IRA1TR 7	12	407	DESS	11° 48.97′ N	117° 30.13′ W
63	SO239, JPIO/CCZ 2015	64	IRA1TR 8	1	419	DESS	11° 48.97′ N	117° 30.13′ W
36	SO268-2, Mining Impact 2	387	DredgeTestArea	11	185	DESS	11° 51.774′ N	117° 00.760′ W
27	SO268-2, Mining Impact 2	307	BGR Reference	9	178	DESS	11° 50.456′ N	117° 03.323′ W
23	SO268-2, Mining Impact 2	244	BGR Reference	4	171	DESS	11° 51.003′ N	117° 03.323′ W
16	SO268-2, Mining Impact 2	250	BGR Reference	9	39	DESS	11° 55.844′ N	117° 01.339′ W
17	SO268-2, Mining Impact 2	267	BGR Trial	8	43	DESS	11° 55.844′ N	117° 01.339′ W
4	SO268-2, Mining Impact 2	32	BGR Trial	6	6	DESS	11° 55.798′ N	117° 01.474′ W

Table 10 List of the kinorhynch ASVs/species detected by metabarcoding in this study, specifying the extraction identification code and the station/area of collection in the CCZ

Extraction Ids and Stations/Areas									
ASV number	Species	4,"158-6"	17,"27-8"	16,"26-9"	23,"40-4"	27,"46-9"	36,"8-11"	63,"IRA56c1"	65,"PRA100c12"
		BGR Trial		BGR Reference				IRA Trial	
4222	*Echinoderes ajax*	0	0	0	0	0	0	0	100
20386	*Echinoderes ajax*	0	0	0	0	0	0	0	0
12177	*Echinoderes ajax*	0	0	0	0	0	0	27	0
18056	*Echinoderes rex*	0	0	0	0	0	0	0	0
8122	*Semnoderes armiger*	2	3	11	0	0	2	0	0
22242	*Semnoderes armiger*	0	0	0	3	0	0	0	0
8233	*Zelinkaderes brightae*	0	0	0	0	0	0	0	0
8793	*Cephalorhyncha sp. HY 2012a*	0	0	0	0	0	0	0	0
8996	*Cephalorhyncha sp. HY 2012a*	0	0	0	0	0	0	0	0
13095	*Cephalorhyncha sp. HY 2012a*	0	0	0	0	0	0	0	5
13156	*Cephalorhyncha sp. HY 2012a*	0	0	0	0	0	0	0	5
13816	*Cephalorhyncha sp. HY 2012a*	0	0	0	0	0	0	0	0
11363	*Condyloderes sp. MVS2014b*	0	0	0	0	0	0	0	0
17043	*Zelinkaderes brightae*	0	0	0	0	3	0	0	0

Extraction Ids and Stations/Areas								
ASV number	Species	58,"IRA43c1"	67,"PRA103c4"	69,"PRA84c12"	72,"PRA87c8"	73,"PRA89c8"	74,"PRA90c11"	121,"IRA1c8"
		IOM			GSR			IRA1
4222	*Echinoderes ajax*	0	0	0	137	0	0	0
20386	*Echinoderes ajax*	0	0	0	5	0	0	0
12177	*Echinoderes ajax*	0	0	0	0	0	0	0
18056	*Echinoderes rex*	0	0	0	0	0	0	0
8122	*Semnoderes armiger*	0	0	48	0	0	0	0
22242	*Semnoderes armiger*	0	0	0	0	0	0	0
8233	*Zelinkaderes brightae*	64	0	0	0	0	0	0
8793	*Cephalorhyncha sp. HY 2012a*	0	0	0	0	0	56	0
8996	*Cephalorhyncha sp. HY 2012a*	0	0	0	0	0	53	0
13095	*Cephalorhyncha sp. HY 2012a*	0	0	0	0	17	0	0
13156	*Cephalorhyncha sp. HY 2012a*	0	0	0	0	17	0	0
13816	*Cephalorhyncha sp. HY 2012a*	0	19	0	0	0	0	0
11363	*Condyloderes sp. MVS2014b*	0	32	0	0	0	0	0
17043	*Zelinkaderes brightae*	0	0	0	0	0	0	7

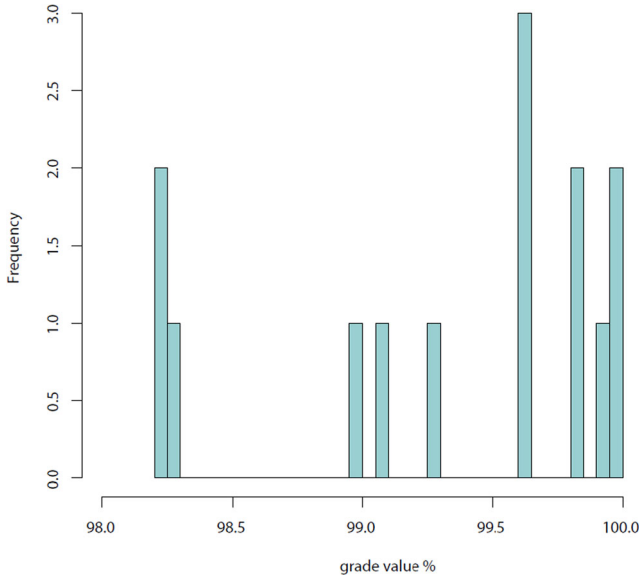

Fig. 15 Histogram of the Grade value from kinorhynch ASVs revealed in the CCZ area. Grade was calculated as a function of blast query coverage and percentage identity (qcov *2 + pident)/3. All ASVs match with grade value of >98% to GenBank

sanctorum sp. nov. being present on segments 4 to 8), and lacks lateroventral spines on segment 9, a feature present in *Echinoderes sanctorum* sp. nov. The presence of these rather uncommon glandular cell outlets on segment 1 was only reported in three additional *Echinoderes* species: *Echinoderes unispinosus* Yamasaki et al., 2018b, *Echinoderes anniae* Sørensen et al., 2018, and *Echinoderes hamiltonorum* Sørensen et al., 2018. However, all of them show additional type 2 glandular cell outlets only on segments 2 and 8, plus on segment 5 in the two former species. The three referred species furthermore have middorsal spines in fewer segments than *Echinoderes sanctorum* sp. nov.: *E. unispinosus* has a single middorsal spine on segment 4, and *E. anniae* and *E. hamiltonorum* on segments 4, 6, and 8 (Sørensen et al. 2018; Yamasaki et al. 2018b).

Echinoderes delaordeni sp. nov. has type 2 glandular cell outlets on segments 2 and 4–9. The four congeners that show most resemblance in this outlet distribution are *Echinoderes multiporus* Yamasaki et al., 2018b, *Echinoderes hwiizaa* Yamasaki & Fujimoto, 2014, *Echinoderes serratulus* Yamasaki, 2016, and *Echinoderes schwieringae* Yamasaki et al., 2019. Of them, *E. multiporus* has the outlets on the same segments as *Echinoderes delaordeni* sp. nov., but may be easily distinguished from the new species by its tergal extensions, which are elongated and spinous-shaped in *E. multiporus* (shortened and distally rounded in *E. delaordeni* sp. nov.), and by the middorsal spine pattern, only present on segments 4, 6, and 8 in *E. multiporus* (Yamasaki et al. 2018b) (throughout segments 4 to 8 in *E. delaordeni* sp. nov.). The remaining three species also show a different middorsal spine pattern: spines completely absent in *E. hwiizaa* (Yamasaki and Fujimoto 2014), spines only present on segment 4 in *E. serratulus* (Yamasaki 2016) and spines on segments 4, 6, and 8 in *E. schwieringae* (Yamasaki et al. 2019). Furthermore, these three species also lack type 2 glandular cell outlets on some of the segments present in *Echinoderes delaordeni* sp. nov.: *E. schwieringae* lacks them on segment 6, and *E. hwiizaa* and *E. serratulus* on segment 9. Finally, *E. hwiizaa* and *E. serratulus* possess ventral glandular cell outlets type 2 on segment 2, instead of the ventral tubes found in *E. delaordeni* sp. nov.

Out of the three new species described herein, *Echinoderes zeppilliae* sp. nov. is the one with the lowest number of type 2 glandular cell outlets, only present on segments 2, 5 and 7–9. The presence of type 2 glandular cells on segments 2, 5, and 8

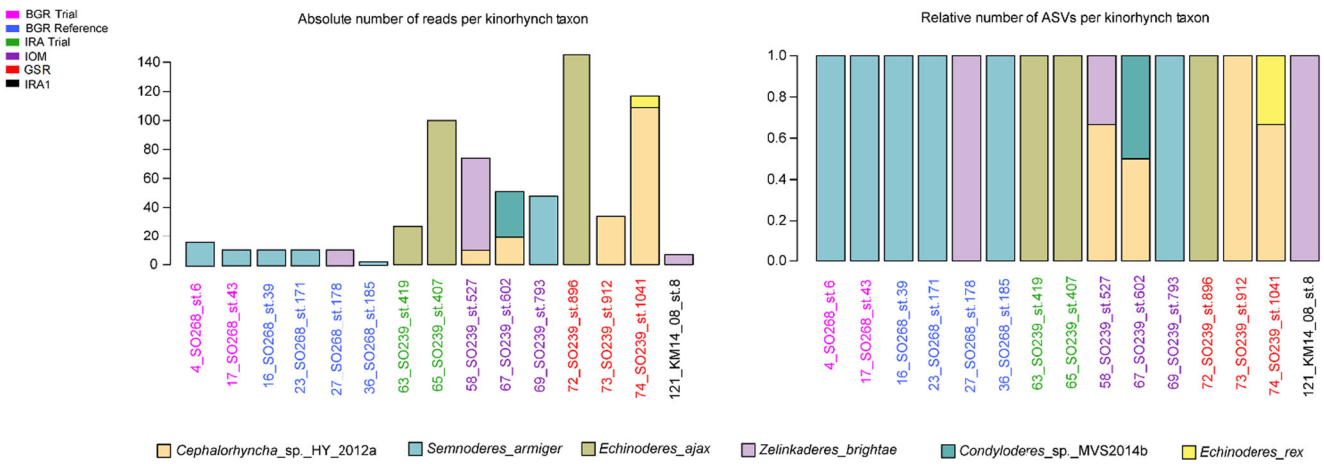

Fig. 16 Barplot showing the absolute number of reads (left) and relative number of ASVs (right) per kinorhynch taxon detected by V1V2 amplicon metabarcoding in the CCZ area. Stations are as shown: Extraction identification number followed by cruise name and station number

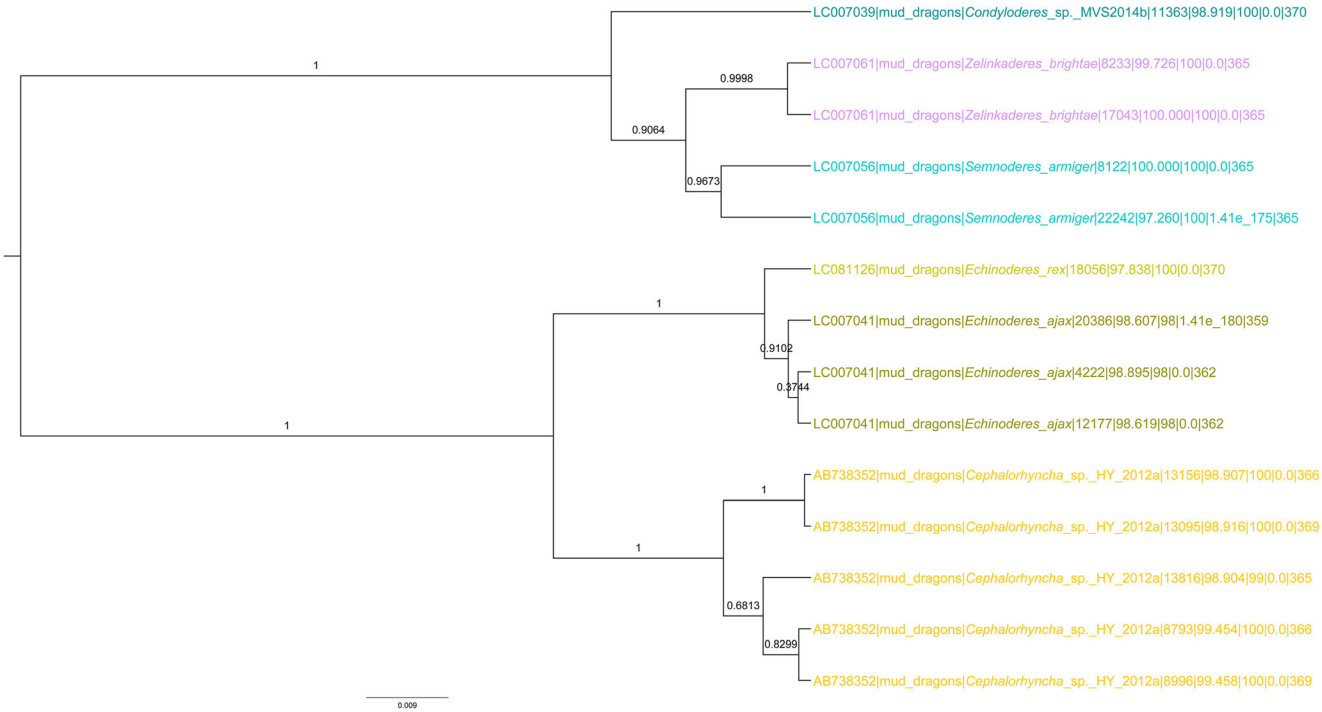

Fig. 17 Phylogram showing well defined clusters of the Kinorhyncha ASVs into species according to the GenBank taxonomic identifications. The numbers on the branches are posterior probabilities and the colors follow the unique species color of barplots in Fig. 16. Taxon labels are accession number followed by taxonomic group, species name, ASV number, percentage identity, query coverage and length of the sequences assigned by blast, retrieved from GenBank

(consequently absent on segments 1, 3–4, and 6) is a relatively common pattern among species with this kind of outlets, shared by *Echinoderes cernunnos* Sørensen et al., 2012, *Echinoderes drogoni* Grzelak & Sørensen, 2018, *Echinoderes romanoi* Landers & Sørensen, 2016, and *Echinoderes xalkutaat* Cepeda et al., 2019a. Nevertheless, only *E. cernunnos* also shows this feature on segment 7 as *E. zeppilliae* sp. nov. (Sørensen et al. 2012). Though, none of the aforementioned species share with *Echinoderes zeppilliae* sp. nov. the presence of the type 2 glandular cell outlets on segment 9. The four mentioned congeners furthermore have more than one pair of these outlets on segment 2 (Cepeda et al. 2019a; Grzelak and Sørensen 2018; Landers and Sørensen 2016; Sørensen et al. 2012), and the new species has not such additional pairs but ventrolateral tubes instead. Additionally, *E. cernunnos* and *E. xalkutaat* also differ from the new species by the presence of elongated, spinous-shaped tergal extensions (Cepeda et al. 2019a; Grzelak and Sørensen 2018; Landers and Sørensen 2016; Sørensen et al. 2012), which are short and distally rounded in *E. zeppilliae* sp. nov.

Regarding the midventral fissure on segment 2 of *Echinoderes zeppilliae* sp. nov., few congeners share the presence of such uncommon feature whose appearance varies with the developmental maturation of a specimen. Consequently, as it becomes only visible in older adults and not in recently hatched specimens, the fissure cannot be used as a useful and reliable diagnostic character to discriminate the new species from those with a similar but weaker feature (*Echinoderes aureus* Adrianov et al., 2002, *Echinoderes setiger* Greeff, 1869, *Echinoderes eximus* Higgins & Kristensen, 1988, *Echinoderes peterseni* Higgins & Kristensen, 1988, *Echinoderes obtuspinosus* Sørensen et al., 2012, and *Echinoderes truncatus* Higgins, 1983) (see Grzelak and Sørensen 2018; Herranz et al. 2017; Neuhaus 2013; Neuhaus and Blasche 2006; Sørensen 2006); or with a more conspicuous fissure (*Echinoderes tubilak* Higgins & Kristensen, 1988, *Echinoderes angustus* Higgins & Kristensen, 1988, *Echinoderes aquilonius* Higgins & Kristensen, 1988, *Echinoderes pennaki* Higgins, 1960) (Grzelak and Sørensen 2018; Herranz et al. 2017; Neuhaus 2013; Neuhaus and Blasche 2006). In any case, the referred species differ from the new one in the lack of ventral tubes on segment 2 and dorsal ones on segment 10, as well as in the pattern of type 2 glandular cells, as their outlets appear on segments 2, 4, 5, and 8 (also on segment 10 for *E. angustus* and *E. aquilonius*).

Even though *Echinoderes zeppilliae* sp. nov., *Echinoderes delaordeni* sp. nov., and *Echinoderes sanctorum* sp. nov. can be easily recognized and discriminated from their congeners by their distribution of middorsal spines and type 2 glandular cell outlets, they also resemble each other in several ways and a detailed discussion focusing on the three new species becomes necessary in order to accomplish proper specimen identifications. Beside the general sensory spot distributions

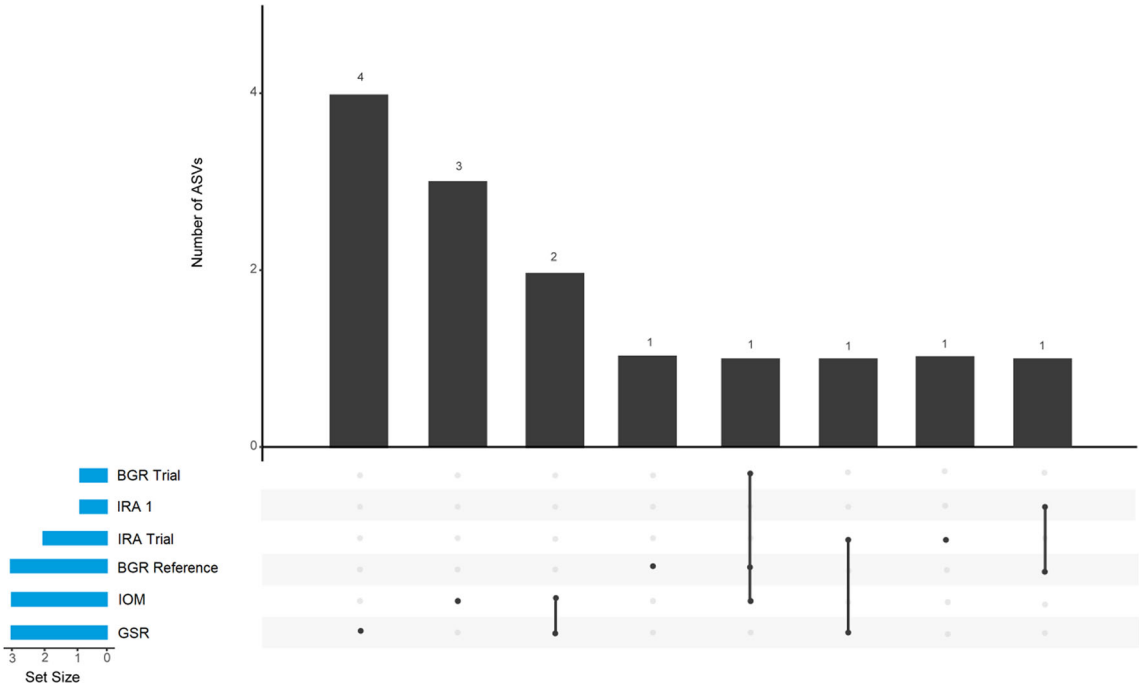

Fig. 18 Upset plot illustrates the intersection of Kinorhyncha ASVs from the CCZ divided into 6 areas of different contractors and cruises. Areas abbreviations on figure are as follows: BGR Reference and Trial area of MiningImpact 2 (BGRRef_SO268 and BGRTial_SO268), Impact Reference Area from MANGAN 2014 (IRA1_Mangan14) and JPIO/CCZ (IRA_Trial_SO239), Global Sea Mineral Resources from JPIO/CCZ (GSR_SO239), and Inter Ocean Metal from JPIO/CCZ (IOM_SO239). Out of the 14 detected ASVs, only four accounted in more than one area

through the trunk, which can exhibit minor intraspecific variation in position and whose observation becomes hard in many cases, there are many other useful features to discriminate between them. First, the pattern of type 2 glandular cell outlets, a feature traditionally used to distinguish among *Echinoderes* species (being even the single mayor character for discrimination between *E. horni* Higgins, 1983 and *E. parahorni* Cepeda et al., 2019b), differs among the three species: on segments 2, 5, 7–9 in *Echinoderes zeppilliae* sp. nov., on segments 2, 4–9 in *Echinoderes delaordeni* sp. nov., and on segments 1–9 in *Echinoderes sanctorum* sp. nov. These patterns are constant for all the specimens of *Echinoderes zeppilliae* sp. nov. and *Echinoderes sanctorum* sp. nov.; although it is true that *Echinoderes delaordeni* sp. nov. shows certain degree of intraspecific variation in the distribution of the referred features, this variability only affects to the bilateral pattern and do not imply the complete lack of the structure on any segment in any specimen, being always present at least in odd number at one side of the tergal plates. Additionally, the rare, consistent dorsal distribution of the type 1 glandular cells in *Echinoderes delaordeni* sp. nov., shifting the position between adjacent segments as a zig-zag alignment (segments 4–7) rather than following the common arrangements present among their congeners and in the other two species described herein, helps in the discrimination of the species. Moreover, there are four additional morphological characters that allow us to distinguish *Echinoderes delaordeni* sp. nov. from *Echinoderes zeppilliae* sp. nov. and *Echinoderes sanctorum* sp. nov. While the last two species show serrated primary pectinated fringes with long tips, a common character among *Echinoderes* species, *Echinoderes delaordeni* sp. nov. has very unique primary pectinate fringes, with marked indentations alternating longer tips and 2-3 shorter tips, giving a frayed appearance to the edge of the segments (the character is consistent between specimens and independent of sampling protocols). Regarding measurements, the spine lengths in *Echinoderes delaordeni* sp. nov. are conspicuously shorter compared to the total trunk length than in the other two new species. This fact is more evident in the middorsal series and toward the posterior segments (see Tables 3, 5, and 7): middorsal spines of segment 7 have a proportion compared to the total trunk length of 9%, while those of *Echinoderes zeppilliae* sp. nov. and *Echinoderes sanctorum* sp. nov. and reach values of 17% and 23%, respectively; middorsal spines of segment 8 have a proportion compared to the total trunk length of 11% in *Echinoderes delaordeni* sp. nov., while those of *Echinoderes zeppilliae* sp. nov. and *Echinoderes sanctorum* sp. nov. and reach values of 24% (twice) and 40% (fourfold), respectively. Moreover, it is noteworthy that *Echinoderes delaordeni* sp. nov., though being the species with the shorter length spine ratio, has the largest laterodorsal tubes on segment 10 (LD10:TL average ratio 16%; *Echinoderes zeppilliae* sp. nov. 11%; and *Echinoderes sanctorum* sp. nov. 7%).

Concerning *Echinoderes sanctorum* sp. nov., as noted above among other characteristics, it can be readily discriminated from its congeners described herein by the presence of larger middorsal spines compared to the total trunk length, a more evident feature toward the posterior trunk segments (MD7:TL average ratio 23%; MD8:TL average ratio 40%). Moreover, out of the three species discussed in this section, females of *Echinoderes sanctorum* sp. nov. and *Echinoderes zeppilliae* sp. nov. show thin and slender lateral terminal accessory spines, more robust in *Echinoderes delaordeni* sp. nov. However, once more, the dimensions of the features help in the morphological identification of the species: *Echinoderes sanctorum* sp. nov. has the largest lateral terminal accessory spines compared to the lateral terminal spines (see Table 5, average ratio 40%), while those of *Echinoderes delaordeni* sp. nov. and *Echinoderes zeppilliae* sp. nov. are 30% (see Tables 3 and 7). Finally, the presence of sensory spots in the lateral series on segments 2–9, except on segment 4, may be useful for the identification of the species, since laterodorsal o midlateral sensory spots are only present on segments 2, 4, 6, 8–9 in *Echinoderes delaordeni* sp. nov.; and on segments 2, 6, 8–9 in *Echinoderes zeppilliae* sp. nov.

The Kinorhyncha community from the CCZ and the Peru Basin

The kinorhynch community of the CCZ is moderately diverse (16 morphologically detected species), but of low density (669 specimens in 254 cores), following the common trends of meiofaunal animals in abyssal plains and in nodule-bearing areas particularly (Glover and Smith 2003; Lambshead et al. 2003). Among the contractor areas, the BGR area is the best studied area by far in terms of sampling effort and hence the higher diversity found there could be expected compared to the other studied areas. Regarding the BGR area, the kinorhynch community is dominated by the family Echinoderidae, which includes two exclusive species (*Echinoderes zeppilliae* sp. nov. and *Echinoderes* sp.6). It is likely that the species absent at the BGR area but found in the other studied contract areas (*Mixtophyes* sp.1, *Centroderes* sp.1, *Condyloderes kurilensis*, and *Echinoderes juliae*) are present here too, but may not have been gathered yet because of their low abundance, since their presence was restricted to only one or two specimens in the UKSR I and GSR areas. Therefore, the kinorhynch community in terms of presence of morphospecies seems quite homogeneous across the CCZ, independently of the contract area.

Agreeing with morphological examinations, metabarcoding data revealed 14 ASVs with low numbers of reads, which further confirms the low density and biomass of kinorhynchs in the manganese nodule area of the CCZ compared to other meiofauna taxa. In line with morphological analyses too, Echinoderidae is the most common family found in genetic analyses, with *Cephalorhyncha* (5 ASVs, detected in IOM and GSR areas) and *Echinoderes* (4 ASVs, present in IOM, GSR, and IRA Trial areas) as the two most common genera. Most of the morphospecies from *Cephalorhyncha* and *Echinoderes* are new and therefore not available in GenBank, which explains why none of them were revealed by metabarcoding analyses at the species level. All the 9 ASVs from these two genera had grade values, between 98.2 and 99.8, which may indicate a low 18S genetic variability between species of kinorhynchs. It is noteworthy that none of the 14 ASVs detected by genetic analyses blasted with the genus *Meristoderes* even though *M. taro* was revealed as the fourth taxa in abundance. This genus is unresolved phylogenetically since it was recovered as a paraphyletic group, with its members nested within *Echinoderes* species (Sørensen et al. 2015). Therefore, one or more ASVs of the *Echinoderes* genus of our data may actually represent *M. taro*. This hypothesis may also be applied to the remaining genus of the family Echinoderidae found only in the morphological records, namely *Fissuroderes*. A single species, *F. higginsi*, was identified in our samples although in low number (four specimens). There are no available sequences in GenBank from this genus, but knowing the unresolved phylogenetic relationships within the family Echinoderidae (Sørensen et al. 2015), the ASVs assigned to *Echinoderes* or *Cephalorhyncha* found in our data may belong to *F. higginsi*. Our argument acquires more strength when comparing both molecular and morphological results since 9 ASVs were assigned to Echinoderidae and 10 morphospecies of Echinoderidae were identified, with two species of the latter group represented by singletons (*E. juliae* and *E.* sp.6) and hence with lower probabilities of being sampled and detected by metabarcoding. Two other taxa identified by genetics, *Semnoderes* and *Condyloderes*, were both recorded by morphology in the CCZ; however, there are no available sequences in GenBank from *S. pacificus* or from *C. kurilensis* to confirm the species-level assignment in metabarcoding. A single specimen from *Centroderes* was found in morphological records but not detected by metabarcoding, most probably due to the rarity of the taxa. The species *Zelinkaderes brightae* Sørensen et al., 2007 revealed by metabarcoding analyses (99.9 grade value, 74 reads and 2 ASVs) was described from the Atlantic Ocean, off Fort Pierce, Florida (Sørensen et al. 2007), and other members of this genus were recorded from the North Sea and Red Sea; however, further analyses are recommended, as neither the species nor the genus have ever been found in the studied area by morphological examination.

Most of the morphospecies and ASVs found in the CCZ appear to have a wide geographic distribution, being present in several contract areas, including *Fissuroderes higginsi*, *Semnoderes pacificus*, *Cephalorhyncha polunga*, *Meristoderes taro*, *Echinoderes delaordeni* sp. nov., *Echinoderes sanctorum* sp. nov., and *Echinoderes* sp. 4. The

last five species, plus *Condyloderes kurilensis* and *Campyloderes* cf. *vanhoeffeni*, were also found in the reference area of the DEA, in the Peru Basin, together with four exclusive, undescribed species (*Antygomonas* sp.1, *Dracoderes* sp.1, *Echinoderes* sp.5, and *Cristaphyes* sp.1). Our findings in the CCZ and the Peru Basin increase the distribution pattern of these species, or fill some gaps in the distribution area across the Pacific Ocean for other ones. *Campyloderes* cf. *vanhoeffeni* was recorded world-wide, from the Faroe Islands to Antarctica (Neuhaus and Sørensen 2013; Zelinka 1913); *Condyloderes kurilensis*, *Echinoderes juliae*, *Fissuroderes higginsi*, and *Semnoderes pacificus* were originally described from the Pacific (*C. kurilensis* from the northwest, see Adrianov and Maiorova 2016; *E. juliae* from USA west coast, see Sørensen et al. 2018; *S. pacificus* and *F. higginsi* from the southwest, see Higgins 1967 and Neuhaus and Blasche 2006); and reported also in deep-sea waters of the Pacific Ocean or at the Caribbean Sea (*F. higginsi* and *C. kurilensis* between southern Oregon and southern California, and *S. pacificus* in Panama; see Sørensen 2006; Sørensen et al. 2018, 2019). Thus, it is not surprising that these species also inhabit the CCZ and/or the Peru Basin according to our results. Although the Peru Basin was not included in the metabarcoding analyses of this study, the occurrence of one species (*Zelinkaderes brightae*) in three defined areas across the CCZ (IOM, BGR Reference, and IRA1) (Fig. 16) can support the hypothesis of the widespread distribution pattern of some kinorhynch species, congruent with morphological analyses of this study and previous records of *Campyloderes* cf. *vanhoeffeni*, *Condyloderes kurilensis*, *E. juliae*, *F. higginsi*, and *S. pacificus* (Adrianov and Maiorova 2016; Neuhaus and Blasche 2006; Neuhaus and Sørensen 2013; Sørensen 2006; Sørensen et al. 2018, 2019).

Significant environmental differences between the GSR, BGR Reference, and IOM areas associated with, for example, total organic carbon, chloro-plastic pigments equivalents, mud content, level of nodule coverage, and/or depth (Macheriotou et al. 2020; Hauquier et al. 2019), may explain the low number of shared ASVs (Fig. 18). Out of the 14 ASVs, four were unique to the GSR and three to the IOM areas, and these two areas shared only two ASVs. None ASV was shared between all the 6 areas and just 4 ASVs occurred in more than one area. A couple of studies have investigated the CCZ meiofauna assemblages using a metabarcoding approach but mainly focused on nematodes, as it is the most abundant group among metazoans (Macheriotou et al. 2020, 2021), or foraminiferans (Lejzerowicz et al. 2021); therefore, no comparison could be provided here in respect to Kinorhyncha. However, among the main results of the referred studies, the authors highlighted the uniqueness of fauna and the significant differences in alpha diversity among the CCZ areas and in comparison with the mid and south Atlantic, northwest Pacific, and southern oceans (Lejzerowicz et al. 2021); a pattern that could be also inferred from the kinorhynch community analyzed in this study.

It is noteworthy to mention the high abundance of juveniles at the CCZ (80%) and the Peru Basin (70%), and the low number of specimens collected from nodules (inhabiting the surface or the crevices). Only one adult specimen of *Cephalorhyncha polunga* and one of *Echinoderes* sp.4 were found in the sediment of washed nodules, whereas the remaining specimens sorted from nodules were juveniles (eight specimens). Nevertheless, specimens of both species were also present in soft sediment samples of the CCZ, which at least for the moment suggests that none of the studied kinorhynch species have a clear preference for nodule habitat. In contrary to the patterns shown by other meiofaunal groups in the CCZ, such as nematodes, that show a lower juvenile proportion than in other deep-sea environments (Gambi et al. 2003; Miljutina et al. 2010), the high proportion of kinorhynch juveniles irrespective of the contract area and the year or season of sampling might point to a reproduction strategy that enables minimization of energetic investment. Due to the food limitation at abyssal depths (Smith et al. 2008b), many meiofauna groups grow slowly and have long life cycles with low energetic expenditure (Seibel and Drazen 2007; Giere 2009), shifting from a "latent" to a "reproductive" community with more juvenile specimens (Ingels et al. 2013). Knowledge on lifecycle duration of kinorhynchs is largely scarce, but the registered kinorhynch densities in our study are worthy of attention in this context. Differences in the total density of kinorhynchs were accompanied by differences in the density of juveniles, although densities of adult specimens were similar between all the contract areas of the CCZ. This fact points to population regulation processes, such as predation or competition for food supply, which could potentially limit the juvenile growth and eventually increase death rates, controlling the adult population size. Conversely, the Peru Basin community had higher survival rates of juveniles, reaching the adult stage and enhancing adult densities compared to the CCZ. Even though food input is one of the main driving factors of abyssal populations at regional to global scale (Smith et al. 2008b), it does not appear to play the decisive role in juvenile survival rates in the exploration contract areas, all located within a mesotrophic zone, and hence with intermediated levels of productivity. Otherwise, the juvenile and adult densities would then be expected to decrease according to the east-to-west drop in sea-surface primary productivity in the CCZ (Bonifácio et al. 2019). This idea must be taken with caution due to the seasonality of the campaigns and the low number of our samples from all the areas, except for the BGR. On the other hand, and even though the low amount of data from the APEI3, the low kinorhynch density found is in line with previous faunistic studies carried out at this oligotrophic area (Bonifácio et al. 2019; Brix et al. 2020), where food supply is minimal and does can negatively affect the total kinorhynch density acting as a

crucial limiting factor, while the kinorhynch density showed higher values in the investigated mesotrophic areas. Considering these facts, APEI3 does not seem to be a proper reservoir either for the kinorhynch community of the studied contractor areas (at least in terms of density), as has also been determined for other fauna groups such as isopods and polychaetes (Bonifácio et al. 2019; Brix et al. 2020). Finally, as already observed in shallow waters by Hoffman et al. (2021), no relation was found between the number of juveniles and gender of the adults that could help clarify the distribution patterns of these communities. Therefore, as is also the case for other meiofaunal groups (Rosli et al. 2018), the kinorhynch communities of the CCZ and the Peru Basin appear to be regulated by a complex mix of biological processes, biotic and abiotic factors that cannot be deciphered due to the relative paucity of adequate data at this stage.

Conclusions

The Clarion-Clipperton Fracture Zone harbors a moderately diverse Kinorhyncha community, with 16 morphologically detected species and 14 ASVs. The high number of singletons at the studied sites likely reflects a diversity underestimation of the whole area and thus new species may be collected during future sampling campaigns. More data from APEI3 or indeed from other APEIs in the CCZ are urgently needed in order to assess the representativeness and accuracy such areas to preserve the biodiversity of the CCZ, including Kinorhyncha. Further investigations combining both morphological and molecular (barcoding) taxonomic approaches from many more samples of all the studied contractor areas would be desirable in order to properly characterize the kinorhynch biodiversity and to estimate the current distribution ranges of the species, since both issues are crucial for the management of deep-sea mining activities.

Supplementary Information There is supplementary information available for this paper https://doi.org/10.1007/s12526-022-01279-z.

Acknowledgements The authors thank Carsten Rühlemann and Thomas Kuhn from Bundesanstalt für Geowissenschaften und Rohstoffe (BGR) in Hannover, who made the material from cruises MANGAN 2010 (R/V Sonne), MANGAN 2013 (R/V Kilo Moana), MANGAN 2014 (R/V Kilo Moana), MANGAN 2016 (R/V Kilo Moana), FLUM (R/V Sonne), and MANGAN 2018 (R/V Sonne) available for this study. Also special thanks to Jens Greinert and Peter Linke from GEOMAR Helmholtz Centre for Ocean Research, Kiel for making available the material from JPIO/DISCOL and MiningImpact 2 cruises. The authors also thank Chris Williams (UKSR) and Craig Smith (University Hawaii) for inviting them to contribute to the Abyssline program. The authors are also in debt to all the participants and the staff involved in the cruises and the staff of the Senckenberg Research Institute, Deutsches Zentrum für Marine Biodiversitätsforschung, Senckenberg am Meer, for sorting the specimens. This manuscript has been associated with record number 81 from the Senckenberg am Meer Metabarcoding and Molecular Laboratory database. We thank Katja Uhlenkott who helped to create the map. We would also like to thank Dr. Birger Neuhaus and the anonymous reviewer for their suggestions and comments that significantly improved the present article.

Funding Open Access funding provided thanks to the CRUE-CSIC agreement with Springer Nature. The EcoResponse cruise (SO239) and SO242 with R/V Sonne were financed by the German Ministry of Education and Science (BMBF) as a contribution to the European project JPI-Oceans (Joint Programming Initiative Oceans) "Ecological Aspects of Deep-Sea Mining" (Contract 03F0707E). The TN-319 (R/V Thomas G. Thompson) cruise was funded by UK Seabed Resources Ltd. (UKSR) and Ocean Minerals Singapore. The authors thank UK Seabed Resources Ltd for providing the necessary funds for the study of the meiofauna from this cruise. NS was funded by the Community of Madrid and the Universidad Complutense de Madrid in the framework of the Research Talent Attraction Programme for incorporation into research groups in the Community of Madrid (2019) (2019-T2/AMB-13328), and DC by a predoctoral fellowship of the Universidad Complutense de Madrid (CT27-16/CT28-16).

Declarations

Conflict of interest The authors declare that they have no conflict of interest.

Ethics approval No approval of research ethics committees was required to accomplish the goals of this study because experimental work was conducted with an unregulated invertebrate species.

Sampling and field studies All necessary permits for sampling and observational field studies have been obtained by the authors from the competent authorities and are mentioned in the acknowledgements.

Data availability All data generated or analyzed during this study are included in this published article and its supplementary information files.

Author contributions PMA, AV, and NS conceived and designed the research. NS identified the specimens. SK and PMA conducted the DNA lab works and analyses for the metabarcoding and wrote this section. NS analyzed and wrote the first draft of the manuscript. NS, AGC, and DC described the new species. FP provided the laboratory facilities to make the morphological study possible. All authors read and approved the manuscript.

References

Adrianov AV, Maiorova AS (2015) *Pycnophyes abyssorum* sp. n. (Kinorhyncha: Homalorhagida), the deepest kinorhynch species described so far. Deep Sea Res Part II Top Stud Oceanogr 111:49–59. https://doi.org/10.1016/j.dsr2.2014.08.009

Adrianov AV, Maiorova AS (2016) *Condyloderes kurilensis* sp. nov. (Kinorhyncha: Cyclorhagida)—a new deep water species from the abyssal plain near the Kuril-Kamchatka. Trench Russ J Mar Biol 42: 11–19. https://doi.org/10.1134/S1063074016010028

Adrianov AV, Maiorova AS (2018a) *Meristoderes okhotensis* sp. nov. – The first deepwater representative of kinorhynchs in the Sea of Okhotsk (Kinorhyncha: Cyclorhagida). Deep Sea Res Part II Top Stud Oceanogr 154:99–105. https://doi.org/10.1016/j.dsr2.2017.10.011

Adrianov AV, Maiorova AS (2018b) *Parasemnoderes intermedius* gen. n. sp. n.—the first abyssal representative of the family Semnoderidae (Kinorhyncha: Cyclorhagida). Russ J Mar Biol 44: 355–362. https://doi.org/10.1134/S1063074018050024

Adrianov AV, Maiorova AS (2019) *Echinoderes ultraabyssalis* sp. nov. from the Kuril-Kamchatka Trench – the first hadal representative of the Kinorhyncha (Kinorhyncha: Cyclorhagida). Prog Oceanogr 178(102142):11. https://doi.org/10.1016/j.pocean.2019.102142

Adrianov AV, Malakhov VV (1999) Cephalorhyncha of the world ocean. KMK Scientific Press, Moscow, p 328

Adrianov AV, Murakami C, Shirayama Y (2002) *Echinoderes aureus* n. sp. (Kinorhyncha: Cyclorhagida) from Tanabe Bay (Honshu Island), Japan, with a key to the genus *Echinoderes*. Spec Div 7(1):47–66. https://doi.org/10.12782/specdiv.7.47

Álvarez-Castillo L, Cepeda D, Pardos F, Rivas G, Rocha-Olivares A (2020) *Echinoderes unispinosus* (Kinorhyncha: Cyclorhagida), a new record from deep-sea sediments in the Gulf of Mexico. Zootaxa 4821(1):196–200. https://doi.org/10.11646/zootaxa.4821.1.13

Amon DJ, Ziegler AF, Dahlgren TG, Glover AG, Goineau A, Gooday AJ, Wiklund H, Smith CR (2016) Insights into the abundance and diversity of abyssal megafauna in a polymetallic-nodule region in the eastern Clarion-Clipperton Zone. Sci Rep 6:30492. https://doi.org/10.1038/srep30492

Blaxter ML, De Ley P, Garey JR et al (1998) A molecular evolutionary framework for the phylum Nematoda. Nature 392:71–75. https://doi.org/10.1038/32160

Bonifácio P, Martínez Arbizu P, Menot L (2019) Alpha and beta diversity patterns of polychaete assemblages across the nodule province of the eastern Clarion-Clipperton Fracture Zone (equatorial Pacific). Biogeosciences 17:865–886. https://doi.org/10.5194/bg-17-865-2020

Brix S, Osborn KJ, Kaiser S, Truskey SB, Schnurr SM, Brenke N, Malyutina M, Martinez Arbizu P (2020) Adult life strategy affects distribution patterns in abyssal isopods—implications for conservation in Pacific nodule areas. Biogeosciences 17:6163–6184. https://doi.org/10.5194/bg-17-6163-2020

Callahan BJ, McMurdie PJ, Rosen MJ, Han AW, Johnson AJ, Holmes SP (2016) DADA2: High-resolution sample inference from Illumina amplicon data. Nat Methods 13:581–583. https://doi.org/10.1038/nmeth.3869

Carman KR, Thistle D, Fleeger JW, Barry JP (2004) Influence of introduced CO2 on deep-sea metazoan meiofauna. J Oceanogr 60:767–772. https://doi.org/10.1007/s10872-004-5769-7

Carus JV (1885) Prodromus Faunae Mediterraneae sive Descriptio Animalium maris Mediterranei incolarum quam comparata silva rerum quatenus innotiut adiectis et nominibus vulgaribus eorumque auctoribus in commodum zoologorum. Vol. I. Coelenterata, Echinodermata, Vermes, Arthropoda. i-xi, 1-525. E. Schweizerbartsche Verlagshandlung E. Koch, Stuttgart

Cepeda D, Álvarez-Castillo L, Hermoso-Salazar M, Sánchez N, Gómez S, Pardos F (2019a) Four new species of Kinorhyncha from the Gulf of California, eastern Pacific Ocean. Zool Anz 282:140–160. https://doi.org/10.1016/j.jcz.2019.05.011

Cepeda D, Sánchez N, Pardos F (2019b) First extensive account of the phylum Kinorhyncha from Haiti and the Dominican Republic (Caribbean Sea), with the description of four new species. Mar Biodivers 49(5):2281–2309. https://doi.org/10.1007/s12526-019-00963-x

Cepeda D, Pardos F, Sánchez N (2021) From biggest to smallest mud dragons: size-latitude trends in a group of meiobenthic animals worldwide. Org Divers Evol 21(1):43–58. https://doi.org/10.1007/s13127-020-00471-y

Clark AL, Clark JC, Pintz S (2013) Towards the development of a regulatory framework for polymetallic nodule exploitation in the Area: note / by the Secretariat publisher, New york 765088:10. http://digitallibrary.un.org/record/765088

Claparède ARE (1863) Zur Kenntnis der Gattung *Echinoderes* Duj. Beobachtungen über Anatomie und Entwicklungsgeschichte wirbelloser Thiere an der Küste von Normandie angestellt. pp. 90–92, 119. Verlag von Wilhelm Engelmann, Leipzig

Gambi C, Vanreusel A, Danovaro R (2003) Biodiversity of nematode assemblages from deep-sea sediments of the Atacama Slope and Trench (South Pacific Ocean). Deep Sea Res I 50:103–117

Giere O (2009) Meiobenthology—the microscopic motile fauna of aquatic sediments, 2nd edn. Springer-Verlag, Berlin

Glover AG, Smith C, Paterson G, Wilson G, Hawkins L, Sheader M (2002) Polychaete species diversity in the central Pacific abyss: local and regional patterns, and relationships with productivity. Mar Ecol Prog Ser 240:157–170. https://doi.org/10.3354/meps240157

Glover AG, Smith CR (2003) The deep-sea floor ecosystem: current status and prospects of anthropogenic change by the year 2025. Environ Conserv 30:219–241. https://doi.org/10.1017/S0376892903000225

Greeff R (1869) Untersuchungen über einige merkwürdige Thiergruppen des Arthropoden- und Wurm-Typus. Archiv fur Naturgeschichte 35: 71–121

Greinert J (2015) RV SONNE SO242-1 DISCOL, Cruise Report / Fahrtbericht, Guayaquil - Guayaquil (Ecuador) 28.07.-25.08.2015, JPI OCEANS ecological aspects of deep-sea mining DISCOL revisited. GEOMAR Helmholtz-Zentrum für Ozeanforschung, Kiel, Germany. https://doi.org/10.3289/GEOMAR_REP_NS_26_2015

Grzelak K, Sørensen MV (2018) New species of *Echinoderes* (Kinorhyncha: Cyclorhagida) from Spitsbergen, with additional information about known Arctic species. Mar Biol Res 14:113–147. https://doi.org/10.1080/17451000.2017.1367096

Grzelak K, Sørensen MV (2019) Diversity and community structure of kinorhynchs around Svalbard: First insights into spatial patterns and environmental drivers. Zool Anz 282:31–43. https://doi.org/10.1016/j.jcz.2019.05.009

Grzelak K, Zeppilli D, Shimabukuro M, Sørensen MV (2021) Hadal Mud Dragons: first insight into the diversity of Kinorhyncha from the Atacama Trench. Front Mar Sci 8:670735. https://doi.org/10.3389/fmars.2021.670735

Ingels J, Vanreusel A, Romano C, Coenjaerts J, Mar Flexas M, Zúñiga D, Martin D (2013) Spatial and temporal infaunal dynamics of the Blanes submarine canyon-slope system (NW Mediterranean); changes in nematode standing stocks, feeding types and gender-life stage ratios. Prog Oceanogr 118:159–174. https://doi.org/10.1016/j.pocean.2013.07.021

Haeckel M, Linke P (2021) RV SONNE Fahrtbericht/Cruise Report SO268—assessing the impacts of nodule mining on the deep-sea environment: nodule monitoring, Manzanillo (Mexico) – Vancouver (Canada), 17.02. – 27.05.2019. GEOMAR Helmholtz-

Zentrum für Ozeanforschung, Kiel, Germany. https://doi.org/10.3289/GEOMAR_REP_NS_59_20.

Halbach P, Fellerer R (1980) The metallic minerals of the Pacific Seafloor. GeoJournal 4(5):407–421 https://www.jstor.org/stable/41142465

Halbach P, Özkara M, Hense J (1975) The influence of metal content on the physical and mineralogical properties of pelagic manganese nodules. Mineral Deposita 10:397–411. https://doi.org/10.1007/BF00207897

Harrell Jr FE (2021) Hmisc: Harrell Miscellaneous. R package version 4.6-0. https://CRAN.R-project.org/package=Hmisc

Hauquier F, Macheriotou L, Bezerra NT, Egho G, Martínez-Arbizu P, Vanreusel A (2019) Distribution of free-living marine nematodes in the Clarion–Clipperton Zone: implications for future deep-sea mining scenarios. Biogeosciences 16:3475–3489. https://doi.org/10.5194/bg-16-3475-2019

Herranz M, Leander BS (2016) Redescription of *Echinoderes ohtsukai* Yamasaki and Kajihara, 2012 and *E. kozloffi* Higgins, 1977 from the northeastern Pacific coast, including the first report of a potential invasive species of kinorhynch. Zool Anz 265:108–126. https://doi.org/10.1016/j.jcz.2016.02.004

Herranz M, Thormar J, Benito J, Sánchez N, Pardos F (2012) *Meristoderes* gen. nov., a new kinorhynch genus, with the description of two new specie and their implications for echinoderid phylogeny (Kinorhyncha: Cyclorhagida, Echinoderidae). Zool Anz 251:161–179. https://doi.org/10.1016/j.jcz.2011.08.004

Herranz M, Yangel E, Leander BS (2017) *Echinoderes hakaiensis* sp. nov.: a new mud dragon (Kinorhyncha, Echinoderidae) from the northeastern Pacific Ocean with the redescription of *Echinoderes pennaki* Higgins, 1960. Mar Biodivers 48:303–325. https://doi.org/10.1007/s12526-017-0726-z

Higgins RP (1960) A new species of *Echinoderes* (Kinorhyncha) from Puget Sound. Trans Am Microsc Soc 79:85–91. https://doi.org/10.2307/3223976

Higgins RP (1967) The Kinorhyncha of New Caledonia. Expédition Française sur les récifs coralliens de la Nouvelle-Calédonie 2:75–90

Higgins RP (1983) The Atlantic barrier reef ecosystem at Carrie Bow Cay, Belize, II. Kinorhyncha. Smithson Contrib Mar Sci 18:1–131. https://doi.org/10.5479/si.01960768.18.1

Higgins RP, Kristensen RM (1988) Kinorhyncha from Disko Island, west Greenland. Smithson Contrib Zool 458:1–56. https://doi.org/10.5479/si.00810282.458

Hoffman KP, Sánchez N, Sørensen MV, Ingels J, Landers SC (2021) Kinorhynch communities of Mobile Bay and the Alabama continental shelf. Cah Biol Mar 62:371–380. https://doi.org/10.21411/CBM.A.B0EA3C57

ISA (2013) ISBA/19/LTC/8 International Seabed Authority, Legal and technical commission. Recommendations for the guidance of contractors for the assessment of the possible environmental impacts arising from exploration for marine minerals in the Area https://www.isa.org.jm/es/documents/isba19ltc8

Janssen A, Kaiser S, Meißner K, Brenke N, Menot L, Martínez Arbizu P (2015) A reverse taxonomic approach to assess macrofaunal distribution patterns in abyssal Pacific polymetallic nodule fields. PLoS One 10:e0117790. https://doi.org/10.1371/journal.pone.0117790

Katoh K, Misawa K, Kuma KI, Miyata T (2002) MAFFT: a novel method for rapid multiple sequence alignment based on fast Fourier transform. Nucleic Acids Res 30:3059–3066. https://doi.org/10.1093/nar/gkf436

Kuhn T (2015) RV SONNE SO240 FLUM, Cruise Report / Fahrtbericht, Manzanillo (Mexico): May 3rd, 2015, Manzanillo (Mexico): June 16th, 2015. Bundesanstalt für Geowissenschaften und Rohstoffe, Hannover, Germany. https://doi.org/10.2312/cr_so240

Lambshead PJD, Brown CJ, Ferrero TJ, Hawkins LE, Smith CR, Mitchell NJ (2003) Biodiversity of nematode assemblages from the region of the Clarion-Clipperton Fracture Zone, an area of commercial mining interest. BMC Ecol 3:1. https://doi.org/10.1186/1472-6785-3-1

Landers SC, Sørensen MV (2016) Two new species of *Echinoderes* (Kinorhyncha, Cyclorhagida), *E. romanoi* sp. n. and *E. joyceae* sp. n., from the Gulf of Mexico. Zookeys 594:51–71. https://doi.org/10.3897/zookeys.594.8623

Lejzerowicz F, Gooday AJ, Barrenechea Angeles I, Cordier T, Morard R, Apothéloz-Perret-Gentil L, Lins L, Menot L, Brandt A, Levin LA, Martinez Arbizu P, Smith CR, Pawlowski J (2021) Eukaryotic biodiversity and spatial patterns in the Clarion-Clipperton Zone and other abyssal regions: insights from sediment DNA and RNA metabarcoding. Front Mar Sci 8:671033. https://doi.org/10.3389/fmars.2021.671033

Lundbye H, Rho HS, Sørensen MV (2011) *Echinoderes rex* n. sp. (Kinorhyncha: Cyclorhagida), the largest *Echinoderes* species found so far. Sci Mar 75(1):41–51. https://doi.org/10.3989/scimar.2011.75n1041

Macheriotou L, Rigaux A, Derycke S, Vanreusel A (2020) Phylogenetic clustering and rarity imply risk of local species extinction in prospective deep-sea mining areas of the Clarion Clipperton Fracture Zone. Proc R Soc B 287:20192666. https://doi.org/10.1098/rspb.2019.2666

Macheriotou L, Rigaux A, Olu K, Zeppilli D, Derycke S, Vanreusel A (2021) Deep-sea nematodes of the Mozambique channel: evidence of random community assembly dynamics in seep sediments. Front Mar Sci 8:549834. https://doi.org/10.3389/fmars.2021.549834

Markhaseva EL, Mohrbeck I, Renz J (2017) Description of *Pseudeuchaeta vulgaris* n sp (Copepoda: Calanoida), a new aetideid species from the deep Pacific Ocean with notes on the biogeography of benthopelagic aetideid calanoids. Mar Biodivers 47:289–297. https://doi.org/10.1007/s12526-016-0527-9

Martínez Arbizu P, Haeckel, M (2015) RV SONNE Fahrtbericht / Cruise Report SO239: EcoResponse Assessing the Ecology, Connectivity and Resilience of Polymetallic Nodule Field Systems, Balboa (Panama) – Manzanillo (Mexico) 11.03.-30.04.2015. GEOMAR Helmholtz-Zentrum für Ozeanforschung, Kiel, Germany, 204 pp. https://doi.org/10.3289/GEOMAR_REP_NS_25_2015

Miljutin DM, Miljutina MA, Martínez Arbizu P, Galéron J (2011) Deep-sea nematode assemblage has not recovered 26 years after experimental mining of polymetallic nodules (Clarion-Clipperton Fracture Zone, Tropical Eastern Pacific). Deep Sea Res Part Oceanogr Res Pap 58:885–897. https://doi.org/10.1016/j.dsr.2011.06.003

Miljutina M, Miljutin D, Mahatma R, Galéron J (2010) Deep-sea nematode assemblages of the Clarion-Clipperton Nodule Province (Tropical North-Eastern Pacific). Mar Biodivers 40:1–15. https://doi.org/10.1007/s12526-009-0029-0

Neuhaus B (2013) Kinorhyncha (= Echinodera). In: Schmidt-Rhaesa A (ed) Handbook of zoology Gastrotricha, Cycloneuralia and Gnathifera, Nematomorpha, vol 1. Priapulida, Kinorhyncha, Loricifera De Gruyter, Berlin, pp 181–348

Neuhaus B (2021) World Kinorhyncha Database. Kinorhyncha. Accessed at: https://www.marinespecies.org/kinorhyncha/aphia.php?p=taxdetails&id=101060 on 2021-11-08

Neuhaus B, Blasche T (2006) *Fissuroderes*, a new genus of Kinorhyncha (Cyclorhagida) from the deep sea and continental shelf of New Zealand and from the continental shelf of Costa Rica. Zool Anz 245:19–52. https://doi.org/10.1016/j.jcz.2006.03.003

Neuhaus B, Sørensen MV (2013) Populations of *Campyloderes* sp (Kinorhyncha, Cyclorhagida): One global species with significant morphological variation? Zool Anz 252:48–75. https://doi.org/10.1016/j.jcz.2012.03.002

Oksanen FJ, Blanchet FG, Kindt R, Legendre P, Minchin PR, O'Hara RB, et al. (2015) vegan: community ecology package. R Package Vegan, Version 2.2-1. Available online at: https://github.com/vegandevs/vegan Accessed 02 October 2019

Paterson GLJ, Wilson GDF, Cosson N, Lamont PA (1998) Hessler and Jumars (1974) revisited: abyssal polychaete assemblages from the Atlantic and Pacific deep sea. Res Part II Top Stud Oceanogr 45: 225–251. https://doi.org/10.1016/S0967-0645(97)00084-2

R Core Team (2020) R: A language and environment for statistical computing. R Foundation for Statistical Computing, Vienna, Austria. http://www.R-project.org/

Rosli N, Leduc D, Rowden A, Robert K (2018) Review of recent trends in ecological studies of deep-sea meiofauna, with focus on patterns and processes at small to regional spatial scales. Mar Biodivers 18: 13–34. https://doi.org/10.1007/s12526-017-0801-5

Rühlemann C, Baumann L, Blöthe M, Bruns A, Eisenhauer A, Georgens R, Hansen J, Heuer L, Kasten S, Kuhn T, Martínez Arbizu P, Milyutina M, Mewes K, Picard A, Rutkowski J, Schott T, Schückel S, Schückel U, Schwarz-Schampera U, Tiltack A, Utecht C, Wöhrl C, Zoch D (2010) Cruise report SO-205 Mangan - Microbiology, paleoceanography and biodiversity in the manganese nodule belt of the Equatorial NE Pacific - Papeete, Tahiti-Manzanillo, Mexico, 14 April - 21 May 2010. Bundesanstalt für Geowissenschaften und Rohstoffe, Hannover, Germany. https://doi.org/10.2312/cr_so205

Rühlemann C, Albers L, Freitag R, Goergens R, Heller C, Janssen A, Kefel O, Kuhn T, Miller J, Ostmann A, Raschka U, Sturm S, Urbaned F, Vink A, Wedemeyer H, Wegorzewski A (2014) RV Kilo Moana MANGAN 2013 Cruise report. Geology and biodiversity of the German Licence area for the exploration of polymetallic nodules in the equatorial NE Pacific Honolulu - Honolulu (Hawaii) 01. April - 13.May.2013. Bundesanstalt für Geowissenschaften und Rohstoffe (BGR), Hannover, Germany

Rühlemann C, Albers L, Gathen M, Goergens R, Heller C, Janssen A, Kaiser S, Kefel O, Kuhn T, Miller J, Mohrbeck I, Perez Calderon D, Raschka U, Mohamed K, Sturm S, Vink A, Wedemeyer H, Wöhrl C (2015) RV Kilo Moana MANGAN 2014 Cruise report. Geology and biodiversity of the German Licence area for the exploration of polymetallic nodules in the equatorial NE Pacific Honolulu - Honolulu (Hawaii) 15. April - 03. June.2014. Bundesanstalt für Geowissenschaften und Rohstoffe (BGR), Hannover, Germany

Rühlemann C, Albers L, Freitag R, Goergens R, Hagedorn D, Halacz J, Heller C, Iwan F, Kefel O, Kuhn T, Miller J, Mohrbeck I, Schumann K, Sturm S, Vink A, Wedemeyer H, Weerts F, Wegorzewski A, Zinßmeister C (2017) RV Kilo Moana MANGAN 2016 Cruise report. Geology and biodiversity of the German Licence area for the exploration of polymetallic nodules in the equatorial NE Pacific Honolulu - Honolulu (Hawaii) 08. April - 20. May.2016. Bundesanstalt für Geowissenschaften und Rohstoffe (BGR), Hannover, Germany

Rühlemann C, Bruns A, Edullantes C, Ercan T, Gatzemeier N, Gillard B, Harbour R, Kefel O, Khodami S, Kuhn T, Nghoongoloka A, Martinez Arbizu P, Menke S, Mercado Salas N, Schmidt K, Sommerfeldt R, Sturm S, Uhlenkot K, Vink A, Wales M, Wedemeyer H, Wegorzewski A, Wöhrl C (2019) RV SONNE MANGAN 2018 Cruise report. Geology and biodiversity of the German Licence area for the exploration of polymetallic nodules in the equatorial NE Pacific Guayaquil (Equador) - Suva (Fiji) 06. April - 29. May.2018. Bundesanstalt für Geowissenschaften und Rohstoffe (BGR), Hannover, Germany

Sánchez N, Pardos F, Sørensen MV (2014a) A new kinorhynch genus, *Mixtophyes* (Kinorhyncha: Homalorhagida), from the Guinea Basin deep-sea, with new data on the family Neocentrophyidae. Helgol Mar Res 68:221–239. https://doi.org/10.1007/s10152-014-0383-6

Sánchez N, Pardos F, Sørensen MV (2014b) Deep-sea Kinorhyncha: two new species from the Guinea Basin, with evaluation of an unusual male feature. Org Divers Evol 14:349–361. https://doi.org/10.1007/s13127-014-0182-6

Sánchez N, Pardos F, Martínez Arbizu P (2019) Deep-sea Kinorhyncha diversity of the polymetallic nodule fields at the Clarion-Clipperton Fracture Zone (CCZ). Zool Anz 282:88–105. https://doi.org/10.1016/j.jcz.2019.05.007

Seibel BA, Drazen JC (2007) The rate of metabolism in marine animals: environmental constraints, ecological demands and energetic opportunities. Philos Trans R Soc B 362:2061–2078. https://doi.org/10.1098/rstb.2007.2101

Shimanaga M, Kitazato H, Shirayama Y (2000) Seasonal patterns of vertical distribution between meiofaunal groups in relation to phytodetritus deposition in the bathyal Sagami Bay, central Japan. J Oceanogr 56:379–387. https://doi.org/10.1023/A:1011120204419

Singh R, Miljutin DM, Vanreusel A, Radziejewska T, Miljutina MM, Tchesunov A, Bussau C, Galtsova V, Martínez Arbizu P (2016) Nematode communities inhabiting the soft deep-sea sediment in polymetallic nodule fields: do they differ from those in the nodule-free abyssal areas? Mar Biol Res 12:345–359. https://doi.org/10.1080/17451000.2016.1148822

Smith CR, Levin LA, Koslow A, Tyler PA, Glover AG (2008a) The near future of the deep-sea floor ecosystems. Aquat Ecosyst Trends Glob Prospects pp. 334–350. https://doi.org/10.1017/CBO9780511751790.030

Smith CR, De Leo FC, Bernardino AF, Sweetman AK, Arbizu PM (2008b) Abyssal food limitation, ecosystem structure and climate change. Trends Ecol Evol 23:518–528. https://doi.org/10.1016/j.tree.2008.05.002

Smith CR, Shipboard Scientific Party (2013) Abyssal baseline study (ABYSSLINE) Cruise Report. Seafloor Investigations Report 2013-1304-051J-SRDL-AB01

Sørensen MV (2006) New Kinorhynchs from Panama, with a discussion of some phylogenetically significant cuticular structures. Meiofauna Mar 15:51–77

Sørensen MV (2008) A new kinorhynch genus from the Antarctic deep sea and a new species of *Cephalorhyncha* from Hawaii (Kinorhyncha: Cyclorhagida: Echinoderidae). Org Divers Evol 8: 230e1–230e18. https://doi.org/10.1016/j.ode.2007.11.003

Sørensen MV (2014) First account of echinoderid kinorhynchs from Brazil, with the description of three new species. Mar Biodivers 44(3):251–274. https://doi.org/10.1007/s12526-013-0181-4

Sørensen MV, Grzelak K (2018) New mud dragons from Svalbard: three new species of *Cristaphyes* and the first Arctic species of *Pycnophyes* (Kinorhyncha: Allomalorhagida: Pycnophyidae). PeerJ 6:e5653. https://doi.org/10.7717/peerj.5653

Sørensen MV, Heiner I, Ziemer O, Neuhaus B (2007) *Tubulideres seminoli* gen. et sp. nov. and *Zelinkaderes brightae* sp. nov. (Kinorhyncha, Cyclorhagida) from Florida. Helgol Mar Res 61: 247–265. https://doi.org/10.1007/s10152-007-0073-8

Sørensen MV, Rho HS, Min WG, Dongsung K, Chang CY (2012) An exploration of *Echinoderes* (Kinorhyncha: Cyclorhagida) in Korean and neighboring waters, with the description of four new species and a redescription of *E. tchefouensis* Lou, 1934. Zootaxa 3368:161–196. https://doi.org/10.11646/zootaxa.3368.1.8

Sørensen MV, Dal Zotto M, Rho HS, Herranz M, Sánchez N, Pardos F, Yamasaki H (2015) Towards a phylogeny of Kinorhyncha, based on morphology and two molecular loci. PLoS One 10:e0133440. https://doi.org/10.1371/journal.pone.0133440

Sørensen MV, Rohal M, Thistle D (2018) Deep-sea Echinoderidae (Kinorhyncha: Cyclorhagida) from the Northwest Pacific. Eur J Taxon 456:1–75. https://doi.org/10.5852/ejt.2018.456

Sørensen MV, Thistle D, Landers SC (2019) North American *Condyloderes* (Kinorhyncha: Cyclorhagida: Kentrorhagata): Female dimorphism suggests moulting among adult *Condyloderes*. Zool Anz 282:232–251. https://doi.org/10.1016/j.jcz.2019.05.015

Yamasaki H (2015) Two new species of *Dracoderes* (Kinorhyncha: Dracoderidae) from the Ryukyu Islands, Japan, with a molecular phylogeny of the genus. Zootaxa 3980:359–378

Yamasaki H, Fujimoto S (2014) Two new species in the *Echinoderes coulli* group (Echinoderidae, Cyclorhagida, Kinorhyncha) from the

Ryukyu Islands, Japan. ZooKeys 382:27–52. https://doi.org/10.3897/zookeys.382.6761 10.11646/zootaxa.3980.3.2

Yamasaki H (2016) Two new *Echinoderes* species (Echinoderidae, Cyclorhagida, Kinorhyncha) from Nha Trang, Vietnam. Zool Stud 55:32. https://doi.org/10.6620/ZS.2016.55-32

Yamasaki H (2021) Hiroshi Yamasaki Website. Study of Meiobenthos – Kinorhyncha, Loricifera, Priapulida, etc. https://sites.google.com/a/meiobenthos.com/laboratory/home?authuser=0 on 2021-04-14

Yamasaki H, Grzelak K, Sørensen MV, Neuhaus B, George KH (2018a) *Echinoderes pterus* sp n showing a geographically and bathymetrically wide distribution pattern on seamounts and on the deep-sea floor in the Arctic Ocean, Atlantic Ocean, and the Mediterranean Sea (Kinorhyncha, Cyclorhagida). ZooKeys 771:15–40. https://doi.org/10.3897/zookeys.771.25534

Yamasaki H, Neuhaus B, George KH (2018b) New species of *Echinoderes* (Kinorhyncha: Cyclorhagida) from Mediterranean seamounts and from the deep-sea floor in the Northeast Atlantic Ocean, including notes on two undescribed species. Zootaxa 4387:541–566. https://doi.org/10.11646/zootaxa.4387.3.8

Yamasaki H, Neuhaus B, George KH (2018c) Three new species of Echinoderidae (Kinorhyncha: Cyclorhagida) from two seamounts and the adjacent deep-sea floor in the Northeast Atlantic Ocean. Cah Biol Mar 59(1):79–106. https://doi.org/10.21411/CBM.A.124081A9

Yamasaki H, Neuhaus B, George KH (2019) Echinoderid mud dragons (Cyclorhagida: Kinorhyncha) from Senghor Seamount (NE Atlantic Ocean) including general discussion of faunistic characters and distribution patterns of seamount kinorhynchs. Zool Anz 282:64–87. https://doi.org/10.1016/j.jcz.2019.05.018

Yoder M, De Ley IT, King IW, Mundo-Ocampo M, Mann J, Blaxter M, Poiras L, De Ley P (2006) DESS: a versatile solution for preserving morphology and extractable DNA of nematodes. Nematology 8:367–376. https://doi.org/10.1163/156854106778493448

Zelinka C (1907) Zur Kenntnis der Echinoderen. Zool Anz 32:130–136

Zelinka C (1928) Monographie der Echinodera. Verlag von Wilhelm Engelmann, Leipzig, pp 1–396